Article

Molecular fate-mapping of serum antibody responses to repeat immunization

https://doi.org/10.1038/s41586-023-05715-3

Received: 29 August 2022

Accepted: 6 January 2023

Published online: 16 January 2023

Check for updates

Ariën Schiepers[1], Marije F. L. van 't Wout[1], Allison J. Greaney[2], Trinity Zang[3], Hiromi Muramatsu[4], Paulo J. C. Lin[5], Ying K. Tam[5], Luka Mesin[1], Tyler N. Starr[2], Paul D. Bieniasz[3,6], Norbert Pardi[4], Jesse D. Bloom[2,6] & Gabriel D. Victora[1]✉

The protective efficacy of serum antibodies results from the interplay of antigen-specific B cell clones of different affinities and specificities. These cellular dynamics underlie serum-level phenomena such as original antigenic sin (OAS)—a proposed propensity of the immune system to rely repeatedly on the first cohort of B cells engaged by an antigenic stimulus when encountering related antigens, in detriment to the induction of de novo responses[1–5]. OAS-type suppression of new, variant-specific antibodies may pose a barrier to vaccination against rapidly evolving viruses such as influenza and SARS-CoV-2[6,7]. Precise measurement of OAS-type suppression is challenging because cellular and temporal origins cannot readily be ascribed to antibodies in circulation; its effect on subsequent antibody responses therefore remains unclear[5,8]. Here we introduce a molecular fate-mapping approach with which serum antibodies derived from specific cohorts of B cells can be differentially detected. We show that serum responses to sequential homologous boosting derive overwhelmingly from primary cohort B cells, while later induction of new antibody responses from naive B cells is strongly suppressed. Such 'primary addiction' decreases sharply as a function of antigenic distance, allowing reimmunization with divergent viral glycoproteins to produce de novo antibody responses targeting epitopes that are absent from the priming variant. Our findings have implications for the understanding of OAS and for the design and testing of vaccines against evolving pathogens.

The ability of serum antibodies to protect against infection is an emergent property of the complex mixture of immunoglobulins secreted over time by B cell clones of various specificities and of a range of affinities. The plasma cells that produce these antibodies arise through multiple parallel pathways, ranging from direct differentiation from naive B cell precursors after primary infection or immunization to elaborate routes involving one or more rounds of affinity maturation in germinal centres (GCs) and intercalating memory B cell phases. The complexity of these cellular pathways compounds markedly with repeated antigenic exposure[9–12], and their ultimate contribution to the serum antibody pool has been difficult to deconvolute. On the one hand, molecular analyses of immunoglobulin genes obtained from memory or GC B cells do not directly assess the composition of antibodies in the serum[13–16]; on the other hand, direct studies of the clonal composition of serum antibody cannot readily assign a cellular or temporal origin to antibodies of different specificities[17,18]. The clonal dynamics of immune phenomena that take place at the serum level therefore remain poorly understood.

A serum-level phenomenon that has been particularly difficult to unravel is OAS, described in the 1950s as a tendency of individuals exposed to a given strain of influenza to respond with antibodies that react more strongly to the first strain of influenza they had met in early childhood than to the exposure strain itself[1,19]. OAS was originally attributed to a propensity of the immune system to repeatedly reuse the first cohort of B cells that respond to an antigen, the reactivity of which will necessarily be biased towards the strain that originally elicited it. However, in contrast to related concepts such as antigenic seniority[4,20], OAS (as defined herein) requires active suppression of the de novo recruitment of new B cell clones from the naive repertoire after boosting[2–4], therefore restricting the ability of the immune system to mount specific antibody responses to escape epitopes. The extent to which this active suppression exists and influences subsequent responses has been debated for decades[5,8]. More recently, B cell fate-mapping experiments in mice have shown that, in apparent contrast to the predictions of OAS, GCs that form in response to boosting consist almost exclusively of naive rather than memory-derived B cells[21–23]. This later addition implies that either the effects of OAS in mice are negligible, or that OAS is a phenomenon that is observed exclusively at the serum level.

Molecular fate-mapping of serum antibody

Resolving this issue, as well as generally understanding the effect of OAS on the response to repeated antigen exposure, would require the ability to transpose such cellular fate-mapping experiments to

[1]Laboratory of Lymphocyte Dynamics, The Rockefeller University, New York, NY, USA. [2]Basic Sciences Division and Computational Biology Program, Fred Hutchinson Cancer Research Center, Seattle, WA, USA. [3]Laboratory of Retrovirology, The Rockefeller University, New York, NY, USA. [4]Department of Microbiology, Perelman School of Medicine, University of Pennsylvania, Philadelphia, PA, USA. [5]Acuitas Therapeutics, Vancouver, British Columbia, Canada. [6]Howard Hughes Medical Institute, Chevy Chase, MD, USA. ✉e-mail: victora@rockefeller.edu

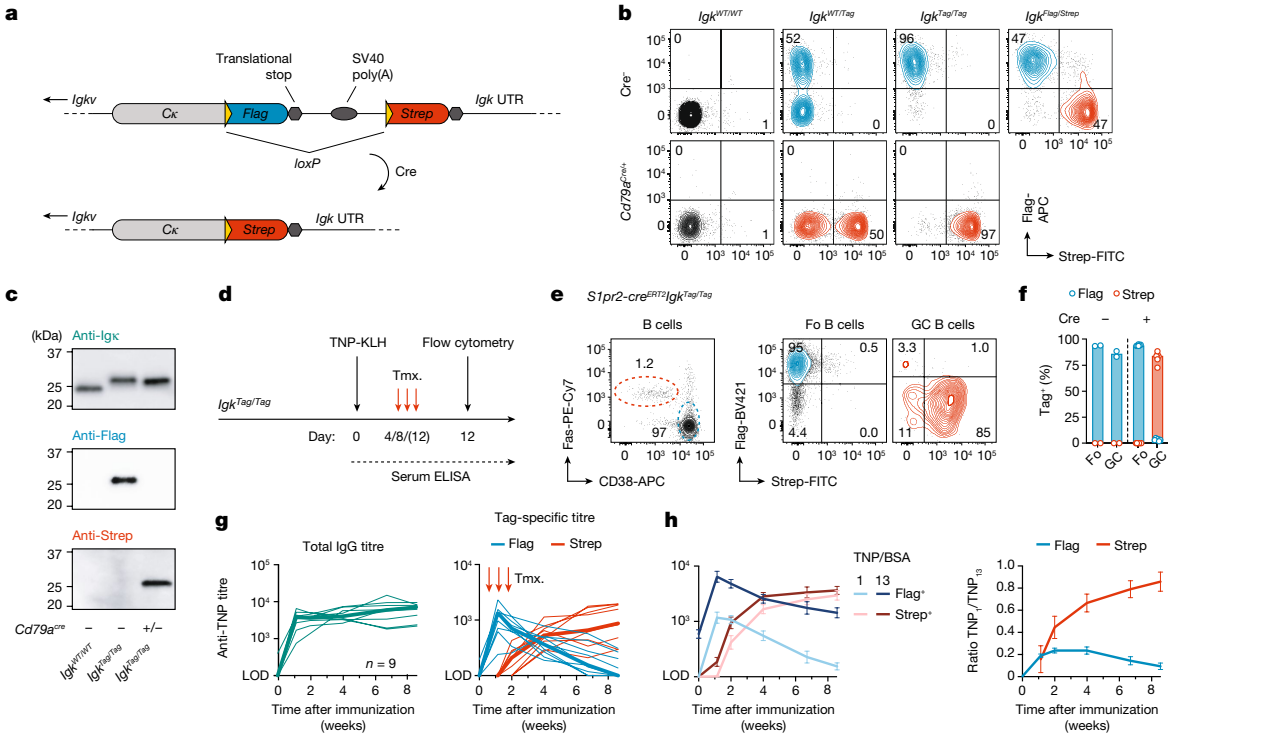

Fig. 1 | The K-tag system for molecular fate-mapping of serum antibodies. **a**, Schematic of the *Igk*^{Tag} (K-tag) allele before and after Cre-mediated recombination. UTR, untranslated region. **b**, Flow cytometry analysis of blood B cells showing the expression of Flag- and Strep-tagged B cell receptors on mice of the indicated genotype. **c**, Western blot analysis of serum obtained from mice of the indicated genotype, stained for Igκ light chain or Flag/Strep tags. Representative of two experiments. **d**, Schematic of the immunization strategy used to fate-map GC B cells and their antibody output. **e**, Flow cytometry analysis of the popliteal lymph node 12 days after footpad immunization with TNP-KLH in alum adjuvant. B cells (B220$^+$CD4$^-$CD8$^-$CD138$^-$) were stained for GC (Fas$^+$CD38$^-$) and follicular (Fo) B cell (Fas$^-$CD38$^+$) markers. **f**, Quantification of the data in **e**. Each dot represents an individual lymph node, and the bars represent the median values. **g**, Anti-TNP total IgG and tag-specific end-point titres as determined by TNP_4-BSA ELISA in mice immunized i.p. with TNP-KLH in alhydrogel adjuvant. The thin lines represent individual mice and the thick lines link the medians of log-transformed titre values at each time point. Results are from nine mice from two independent experiments. Tmx., tamoxifen. **h**, The relative affinity of anti-TNP Flag$^+$ and Strep$^+$ antibodies of the same samples shown in **g** as estimated by ELISA using TNP_1-BSA or TNP_{13}-BSA as capture reagents. Data are mean ± s.e.m. of the log-transformed titre values. The ratio between anti-TNP_1-BSA and anti-TNP_{13}-BSA titres was calculated per sample, shown on the right.

the serum antibody itself. To achieve this, we adapted the classic fate-mapping strategy to enable the detection of the cellular and temporal origin of antibodies in the serum—an approach that we call molecular fate-mapping. We engineered mice in which the C terminus of the immunoglobulin kappa (Igκ) light chain gene (*Igk*) is extended to encode a LoxP-flanked Flag tag, followed by a downstream Strep tag (Fig. 1a and Extended Data Fig. 1). B cells bearing this 'K-tag' allele produce immunoglobulins that are Flag-tagged unless they are exposed to Cre recombinase, after which they permanently switch the Flag tag for a Strep tag. Cre-mediated recombination therefore fate-maps the antibodies that these B cells and their plasma cell descendants express on their surfaces and/or secrete into serum. This enables differential detection of pre- and post-fate-mapping Igκ$^+$ antibodies using secondary reagents specific for each tag.

To verify the functionality of the K-tag allele, we first determined that B cells in *Igk*^{Tag} mice expressed tagged B cell receptors on their surface. Following the rules of allelic exclusion[24], around 50% and 95% of B cells from mice expressing heterozygous *Igk* (wild type (WT)/tag) or homozygous *Igk*$^{Tag/Tag}$ mice were Flag$^+$ (as expected, about 5% of B cells in homozygous mice carried an Igλ light chain[24]; Extended Data Fig. 2a). K-tag mice in which all B cells constitutively expressed Cre recombinase (*Igk*$^{Tag/Tag}$*Cd79a*$^{Cre/+}$) replaced Flag with a Strep tag in almost all Igκ$^+$ B cells (Fig. 1b). Importantly, K-tag mice appropriately secreted Flag- or Strep-tagged antibodies into the serum in the absence or presence of Cre recombinase, respectively (Fig. 1c), without affecting steady-state serum antibody levels (Extended Data Fig. 2b). The generation and maturation of K-tag B cells was unimpaired, as indicated by the equal proportion of tagged and untagged circulating B cells in *Igk*$^{WT/Tag}$ mice (Fig. 1b). The same was true of circulating B cells and bone marrow plasma cells expressing Flag and Strep tags in *Igk*$^{Flag/Strep}$ mice, in which one of the two K-tag alleles was prerecombined by Cre expression in the germline (Fig. 1b and Extended Data Fig. 2c).

To ensure that Flag$^+$ and Strep$^+$ B cells were equally competitive throughout the course of B cell activation, affinity maturation and plasma cell differentiation, we primed and boosted *Igk*$^{Flag/Strep}$ mice with the model antigen 2,4,6-trinitrophenyl-keyhole limpet haemocyanin (TNP-KLH) in alum adjuvant and followed the serum titres of antibodies bearing each tag over time. To enable a direct comparison of titres of anti-TNP antibodies bearing each tag, we diluted secondary (anti-Flag or anti-Strep) antibodies to achieve similar detection of standard curves generated using recombinant Flag- or Strep-tagged monoclonal antibodies (Extended Data Fig. 2d). End-point enzyme-linked immunosorbent assay (ELISA) titres normalized using these curves showed a similar range of anti-TNP reactivity between the Flag$^+$ and Strep$^+$ fractions (Extended Data Fig. 2e), indicative of equal competitiveness of the differently tagged B cells.

Following the serum antibody produced by B cells engaged at different stages of the immune response requires temporally restricted fate-mapping of activated B cell clones. To enable this, we crossed *Igk*^{Tag} mice to the GC-specific, tamoxifen-inducible *S1pr2-cre*^{ERT2} BAC-transgenic allele[25] (to generate *S1pr2-Igk*^{Tag} mice). Tamoxifen treatment of mice on days 4 and 8 after TNP-KLH immunization led

to efficient recombination (96.1 ± 0.50% (mean ± s.e.m.) ((Strep$^+$/Tag$^+$) × 100)) of the K-tag allele in GC B cells but not in non-GC B cells in the same lymph node at 12 days after immunization (d.p.i.) (Fig. 1d–f). Again, tagged B cells were found at similar proportions to untagged B cells in heterozygous *S1pr2-Igk*$^{WT/Tag}$ mice (on average 41 ± 9.0% (mean ± s.d.) Tag$^+$), indicating that expression of the tag does not impair B cell competitiveness in the GC (Extended Data Fig. 2f,g). GC B cells in Cre$^-$ animals (Fig. 1f) or *S1pr2-Igk*$^{WT/Tag}$ mice not treated with tamoxifen remained Flag$^+$, with only minimal spontaneous recombination (1.3 ± 1.0% (mean ± s.d.) Strep$^+$ at day 12 d.p.i.) in the latter (Extended Data Fig. 2g).

Total anti-TNP IgG antibodies in *S1pr2-Igk*^{Tag} mice immunized intraperitoneally (i.p.) with TNP-KLH in alhydrogel and treated with tamoxifen on days 4, 8 and 12 were first detected in the serum at 8 d.p.i. and increased progressively until 60 d.p.i. (Fig. 1g). Deconvolution of GC-derived (Strep$^+$) and non-GC derived (Flag$^+$) antibodies showed that an initial wave of extrafollicular Flag$^+$ antibodies that peaked at 8 d.p.i. was progressively replaced by GC-derived Strep$^+$ antibodies that were first detected in the serum at 14 d.p.i. (Fig. 1g). Flag$^+$ anti-TNP antibodies regressed to near baseline levels between 47–60 d.p.i., as expected from their extrafollicular origin. An affinity-dependent anti-TNP ELISA showed detectable affinity maturation only in the GC-derived Strep$^+$ antibody fraction (Fig. 1h), confirming the efficient fate-mapping of GC-derived antibody. The background signal in control animals that were not given tamoxifen remained below the limit of detection (LOD) throughout the primary response (Extended Data Fig. 2h). Thus, the *S1pr2-Igk*^{Tag} mouse model enables us to discern antibodies derived from the first wave of B cells that entered a GC reaction in response to immunization. Our data also show that extrafollicular responses are of relatively short duration in these settings and that almost all antibodies detectable after the first few weeks of immunization, and especially antibodies with high affinity, were derived from plasma cells of GC origin.

Primary addiction in homologous boosting

With this system in hand, we sought to measure the extent to which OAS-type suppression affects the development of de novo antibody responses to homologous boosting (we refer to this suppression generically as primary addiction, to encompass the homologous regimen). To this end, we took advantage of the ability to trigger Cre-mediated recombination of the K-tag allele in a time-resolved manner by administration of tamoxifen to mark serum antibodies produced by B cells that formed GCs in response to primary immunization (the primary cohort). In addition to labelling primary-cohort B cells, this approach also 'reverse fate-maps' with a Flag tag any antibodies that arose from clones engaged de novo by subsequent booster doses. This property enables us to distinguish between two models of recall antibody response: (1) a simple sequential contribution model, in which de novo responses, although smaller than memory-derived ones, are nevertheless allowed to progress with similar kinetics to a new primary response, adding up as more doses of antigen are provided (related to antigenic seniority); and (2) a primary addiction model (related to OAS), in which the primary response actively suppresses the emergence of subsequent de novo antibody responses even after several boosts (Fig. 2a).

We primed *S1pr2-Igk*^{Tag} mice i.p. with alum-adjuvanted TNP-KLH and administered tamoxifen at 4, 8 and 12 d.p.i. to fate-map the primary cohort GC B cells and their memory and plasma cell progeny (Fig. 2b). In this setting, all primary-cohort-derived antibodies are Strep$^+$, whereas any antibody produced by B cell clones expanded de novo by secondary or higher-order boosting (including by their memory or plasma cell progeny) will be reverse fate-mapped as Flag$^+$. Importantly, as we do not rely on differences between antigen variants to distinguish primary from secondary or later antibodies, this approach enables us to measure primary addiction at zero-antigenic distance—that is, when priming and boosting with the exact same antigen. As suppression of de novo antibody responses is likely to decrease as antigenic distance increases[26,27], this approach enables us to estimate the strength of primary addiction when it is at its strongest.

Homologous boosting 1 and 2 months after the primary immunization resulted in the expected increases in recall TNP titres (Fig. 2c) and the formation of recall GCs that were dominated by naive-derived B cells[21] (Extended Data Fig. 3a). Deconvolution of these responses using tag-specific ELISA revealed that both secondary and tertiary titres were strongly dominated by fate-mapped (Strep$^+$) antibodies derived from primary cohort B cells. Whereas Flag$^+$ TNP-specific antibodies also appeared after each boost, their titres peaked at much lower levels and decayed markedly with time (Fig. 2c). Importantly, counter to the expectations of the sequential contribution model (Fig. 2a), Flag$^+$ titres did not increase progressively between the second and third antigen doses, when any Flag$^+$ memory B cells would have been reactivated. To synthesize both measures, we created a 'primary addiction index', computed by dividing Strep$^+$ by total Strep$^+$ + Flag$^+$ titres ($S/(S+F) \times 100$). This showed that almost all detectable recall antibodies (mean 95% and 97% of serum reactivity at 14 days after the first and second boosts, respectively) were derived from the B cell cohort engaged in the primary GC response (Fig. 2d). Depletion of IgM from serum samples after boosting resulted in a sharp reduction in Flag$^+$ but not Strep$^+$ recall TNP titres, supporting the notion that naive-derived B cells engaged by recall generate primarily an extrafollicular-like (IgM-dominated) B cell response (Extended Data Fig. 3b,c).

To extend these findings to a clinically relevant setting, we immunized and boosted mice as in Fig. 2b but using a lipid nanoparticle (LNP)-formulated nucleoside-modified mRNA vaccine encoding the prefusion-stabilized (2P) form of the SARS-CoV-2 Wuhan-Hu-1 (WH1) spike (S) protein, similar to available SARS-CoV-2 mRNA vaccines[28]. Secondary and tertiary anti-S protein receptor-binding domain (RBD) antibodies were again almost entirely derived from primary cohort (Strep$^+$) B cells (Fig. 2e,f). As with GC B cells (Extended Data Fig. 2g), low-level spontaneous recombination to Strep$^+$ antibodies was detected in recall responses in control mice not given tamoxifen. This resulted in a slight underestimation of Flag$^+$ antibody titres (median 2.1% and 2.8% 2 weeks after second and third immunizations, respectively; Extended Data Fig. 3d). Although primary addiction was more pronounced for the SARS-CoV-2 RBD than for TNP-KLH after the first boost (no new (Flag$^+$) antibody was detected at this time point), 5 out of 12 mice developed low but stable titres of Flag$^+$ anti-RBD antibodies after the third dose. This bimodality was independent of the experimental cohort and of whether boosting was done ipsilaterally or contralaterally to the site of the primary dose (Extended Data Fig. 3e) and is therefore likely ascribable to stochastic variability inherent to highly oligoclonal recall responses[21]. To quantify the extent to which de novo antibody responses to the boost were suppressed by previous priming (that is, the magnitude of the primary addiction suppressive effect), we compared Flag$^+$ antibodies in mice that were given three doses of WH1 mRNA–LNPs (WWW) to an additional group in which the priming and fate-mapping steps were omitted (ØWW). Flag$^+$ responses were 55-fold lower in WWW mice compared with in ØWW mice at 4 weeks after the final dose (Fig. 2g), indicating strong suppression of new B cell responses in primed animals compared with what they would have been in the absence of priming. Finally, primary addiction was long lasting, as even a fourth immunization of a subset of mice (>133 days after the previous boost) was dominated by Strep-tagged antibodies (Fig. 2h and Extended Data Fig. 3f), again failing to demonstrate the progressive increase in Flag$^+$ antibody titres predicted by a simple sequential contribution model (Fig. 2a). We conclude that primary addiction can be very strong when measured at zero antigenic distance—evidence of OAS-type suppression of de novo B cell responses by pre-existing immunity.

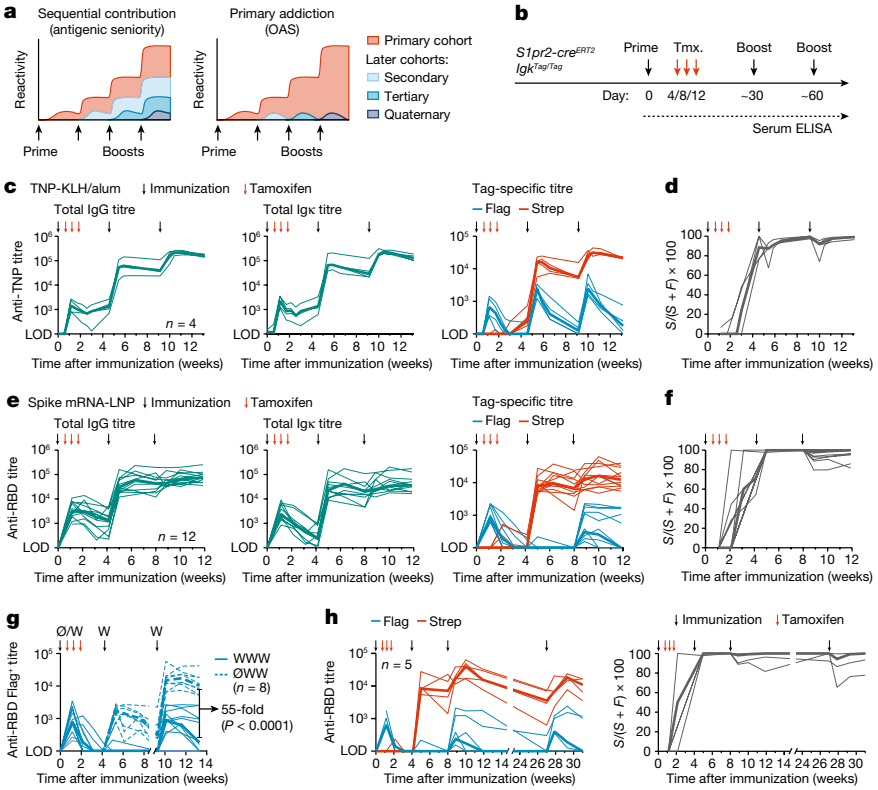

Fig. 2 | Primary addiction after homologous boosting. a, Schematic of the sequential contribution and primary addiction models of antigenic imprinting. **b**, The general immunization strategy used to measure primary addiction. *S1pr2-Igk*$^{Tag/Tag}$ mice were immunized on the days indicated by black arrows with TNP-KLH in alum (**c**,**d**) or WH1 mRNA–LNP (**e**–**g**) and treated with tamoxifen at 4, 8 and 12 d.p.i. as indicated by the red arrows. **c**, Anti-TNP serum IgG (left), Igκ (middle) and tag-specific titres (right) as measured using TNP_4-BSA by ELISA. The results are from four mice from two independent experiments. The thin lines represent individual mice and the thick lines link the medians of log-transformed titre values at each timepoint. **d**, The percentage of the TNP titre derived from the primary cohort of B cells (the primary addiction index) was calculated by dividing the Strep$^+$ titre of each individual sample by its total titre (Strep$^+$ + Flag$^+$), multiplied by 100 ($S/(S+F) \times 100$). **e**, Anti-WH1 RBD IgG (left), Igκ (middle) and tag-specific titres (right) as measured by ELISA. Results are from 12 mice from 3 independent experiments. **f**, The primary addiction index was calculated as described in **d**. **g**, Comparison of de novo Flag$^+$ antibody responses in the presence or absence of primary immunization. WWW, three doses of WH1 S mRNA; ØWW, first dose and fate-mapping omitted. WWW data are for the same samples as in **e**, remeasured in the same assay as ØWW. **h**, The quaternary anti-WH1 RBD response (left) and primary addiction index (right) in mice that received a fourth dose of mRNA–LNP at 133 days after the previous dose, for one of the cohorts shown in **e**. Two out of the five mice were not sampled at day 0.

Antigenic drift limits primary addiction

To measure how primary addiction responds to increases in antigenic distance between priming and boosting antigens, we used historical series of drifted influenza virus haemagglutinin (HA) variants as models. We first used an influenza infection/immunization model (Fig. 3a) based on two of the strains for which OAS was originally described—A/Puerto Rico/8/1934 (PR8) and A/Fort Monmouth/1/1947 (FM1)[1,19]—of which the HAs (HA_{PR8} and HA_{FM1}) share 90% identity at the amino acid level (Fig. 3b). As with hapten and mRNA immunization, the primary response to HA_{PR8} was characterized by high extrafollicular (Flag$^+$) titres that peaked between 8 and 16 days after infection and were subsequently replaced by GC-derived (Strep$^+$) titres (Fig. 3c). Homologous boosting with recombinant HA_{PR8} protein subcutaneously at 3 and 4 months after infection resulted in a 1 log increase in Strep$^+$ HA_{PR8} binding titres after the first boost and a less pronounced increase after the second boost. As with protein immunization, the contribution of non-primary (Flag$^+$) antibodies to total titres was small—even though it increased progressively between the first and second boosts, its peak median value was around 10% of HA reactivity (Fig. 3c). Heterologous boosting with HA_{FM1} led to only slight back-boosting of primary Strep$^+$ HA_{PR8} titres and had almost no effect on Flag$^+$ HA_{PR8} reactivity (Fig. 3d), indicative of substantial antigenic distance between these variants. Accordingly, cross-reactive primary titres towards HA_{FM1} were completely absent from the primary extrafollicular response to PR8 infection and began to emerge only at approximately 4 weeks in the Strep$^+$ antibody fraction (Fig. 3d), probably as a side effect of affinity maturation towards HA_{PR8}. Heterologous boosting not only increased these cross-reactive (Strep$^+$) titres by close to 1 log but, importantly, also induced substantial responses from de novo clones elicited by the boost, in that around half of all serum reactivity to HA_{FM1} was derived from the Flag$^+$ fraction after the second boost (Fig. 3d). Comparing these levels to those achieved by two doses of HA_{FM1} in the absence of previous infection showed that primary addiction suppressed new responses by 3.8-fold (Extended Data Fig. 4a), much less than the 55-fold suppression achieved in homologous mRNA-vaccination (Fig. 2g). Thus, heterologous boosting partly circumvents primary addiction, enabling improved expansion and serum contribution of variant-specific B cell clones that are not involved in the primary response.

To verify this notion over a wider range of antigenic distances, we immunized mice i.p. with recombinant H1 from strain A/New York/614/1995 (HA_{NY95}) in alhydrogel adjuvant, then boosted these mice twice, either homologously with HA_{NY95} or heterologously with H1s from strains A/New Caledonia/20/1999 (HA_{NC99}; a slightly drifted strain with 96% amino acid identity to HA_{NY95}) or pandemic A/California/07/2009 (HA_{CA09}; an 'antigenic shift' strain, with 80% amino acid identity; Fig. 3e and Extended Data Fig. 4b). Generally, primary addiction was weaker

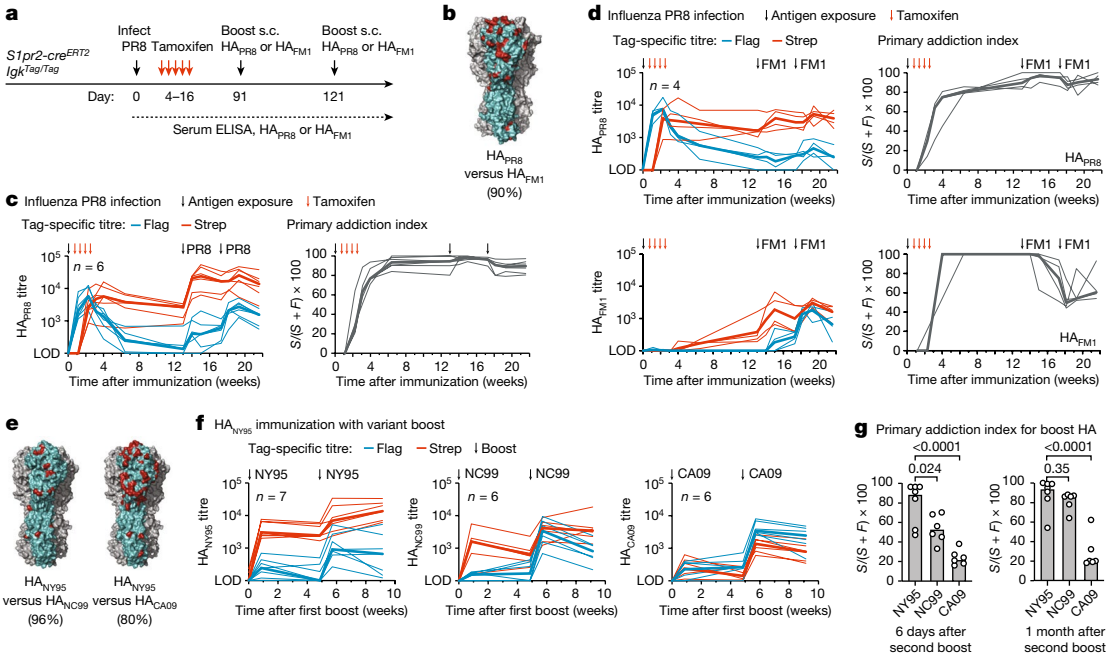

Fig. 3 | Primary addiction decreases with antigenic distance. a, Schematic of the influenza infection and HA boosting strategy. *S1pr2-Igk*$^{Tag/Tag}$ mice were infected intranasally with PR8 influenza and boosted subcutaneously (s.c.) with HA_{PR8} or HA_{FM1} in alhydrogel at the indicated time points. **b**, Rendering of the HA_{PR8} trimer structure (Protein Data Bank (PDB): 1RU7) with one monomer highlighted in teal and the amino acids that diverge between HA_{PR8} and HA_{FM1} in red. The percentage amino acid identity is shown in parentheses. **c**, Anti-HA_{PR8} Flag$^+$ and Strep$^+$ titres in *S1pr2-Igk*$^{Tag/Tag}$ mice that were homologously boosted with HA_{PR8} (left) and quantification of the primary addiction index score (right). **d**, Anti-HA_{PR8} (top) and anti-HA_{FM1} (bottom) ELISA reactivity in mice that were heterologously boosted with HA_{FM1}. Tag-specific titres (left) and quantification of the primary addiction index (right) are shown. **e**, The divergence between HA_{NC95} and HA_{NC99} or HA_{CA09}, coloured as in **b**. Modelled on the structure of HA_{CA09} (PDB: 3LZG). **f**, Anti-HA tag-specific titres in mice primed with HA_{NY95} protein, shown after the first boost with HA_{NY95} (homologous) or with variants HA_{NC99} or HA_{CA09} (heterologous), as outlined in Extended Data Fig. 4b. Antibody reactivity to the boosting antigen is shown. The full time-course and reactivities against all three HAs as measured by ELISA for the top serum dilution are shown in Extended Data Fig. 4c. **g**, Primary addiction index for the boosting HA, 6 days (left) and 1 month (right) after the second boost (third dose). *P* values were calculated using two-tailed Student's *t*-tests, comparing the primary addiction index of the homologous to each heterologous boost. The thin lines represent individual mice and the thick lines link medians of log-transformed titre values at each time point. All of the results are from two independent experiments, with the number of mice in each group indicated in the graphs.

and more variable in this setting, even with homologous boosting, possibly due to the overall weak primary response elicited by recombinant HA_{PR8} protein (Extended Data Fig. 4c). Nevertheless, we observed a progressive decrease in primary addiction as the antigenic distance between the primary and boost antigens increased, so that up to 80% of total serum responses to HA_{CA09} were Flag-tagged (corresponding to 20% primary addiction) after boosting with this variant (Fig. 3f,g). Pooling data for the infection and immunization experiments according to the similarity between priming and boosting HAs showed a highly significant linear decrease in primary addiction as antigenic distance increased (Extended Data Fig. 4d). We conclude that increased antigenic distance between priming and boosting antigens counteracts primary addiction, therefore enabling the generation of new, variant-specific antibody responses.

Heterologous SARS-CoV-2 spike boosting

A setting in which subversion of primary addiction by antigenic distance is clinically important is the response to Omicron strains of SARS-CoV-2 in individuals who were previously exposed to antigens from the WH1 strain. We used the K-tag system to estimate the degree to which boosting with mRNA–LNP encoding the S protein from the Omicron BA.1 strain was capable of overcoming primary addiction generated by priming with WH1-S-encoding mRNA–LNP (the WH1 and BA.1 strains have 98% and 92% amino acid identity in the full S protein and RBD domains, respectively). We primed *S1pr2-Igk*^{Tag} mice with WH1 mRNA–LNP in the right leg, then boosted these mice 1 and 2 months later with either BA.1 or WH1 mRNA–LNP distally in the left leg (Fig. 4a). Boosting induced similar total IgG responses to WH1 and BA.1 RBDs in both groups (Fig. 4b). By contrast, whereas sera from both groups neutralized a WH1 pseudovirus[29] equally, BA.1-boosted serum was on average 15-fold more potent against BA.1 pseudovirus, indicating a strong qualitative difference between the heterologous and homologous boosting regimens. Deconvolution of these effects by tag-specific ELISA revealed responses to the WH1 RBD that were indistinguishable between homologously and heterologously boosted animals, in that primary (Strep$^+$) antibodies were strongly dominant in both settings, with no substantial Flag$^+$ response after the initial extrafollicular response (Fig. 4c,d). Whereas little to no Strep$^+$ antibodies to the BA.1 RBD were observed after primary immunization, recall Strep$^+$ reactivity to the BA.1 RBD was equally strong regardless of which variant was used for boosting (Fig. 4c,d). This observation agrees with previous reports documenting the evolution of cross-reactivity to other strains as a consequence of affinity maturation towards WH1 vaccination in humans[30]. Importantly, however, heterologous boosting resulted in a pronounced increase in BA.1 RBD titres generated by newly recruited (Flag$^+$) clones that were not cross-reactive with the WH1 strain, a reactivity otherwise absent from mice boosted homologously (Fig. 4c,d). At their peak (2 weeks after the second boost), Strep$^+$ antibodies accounted for an average of 73% (±19% s.d.) of total anti-BA.1 reactivity across heterologously boosted mice (Fig. 4d). The induction of new (Flag$^+$) antibodies after double BA.1 boost was even more pronounced when assaying for reactivity against the full-length WH1 and BA.1 S proteins (Fig. 4e). Two doses of BA.1 in the absence of previous

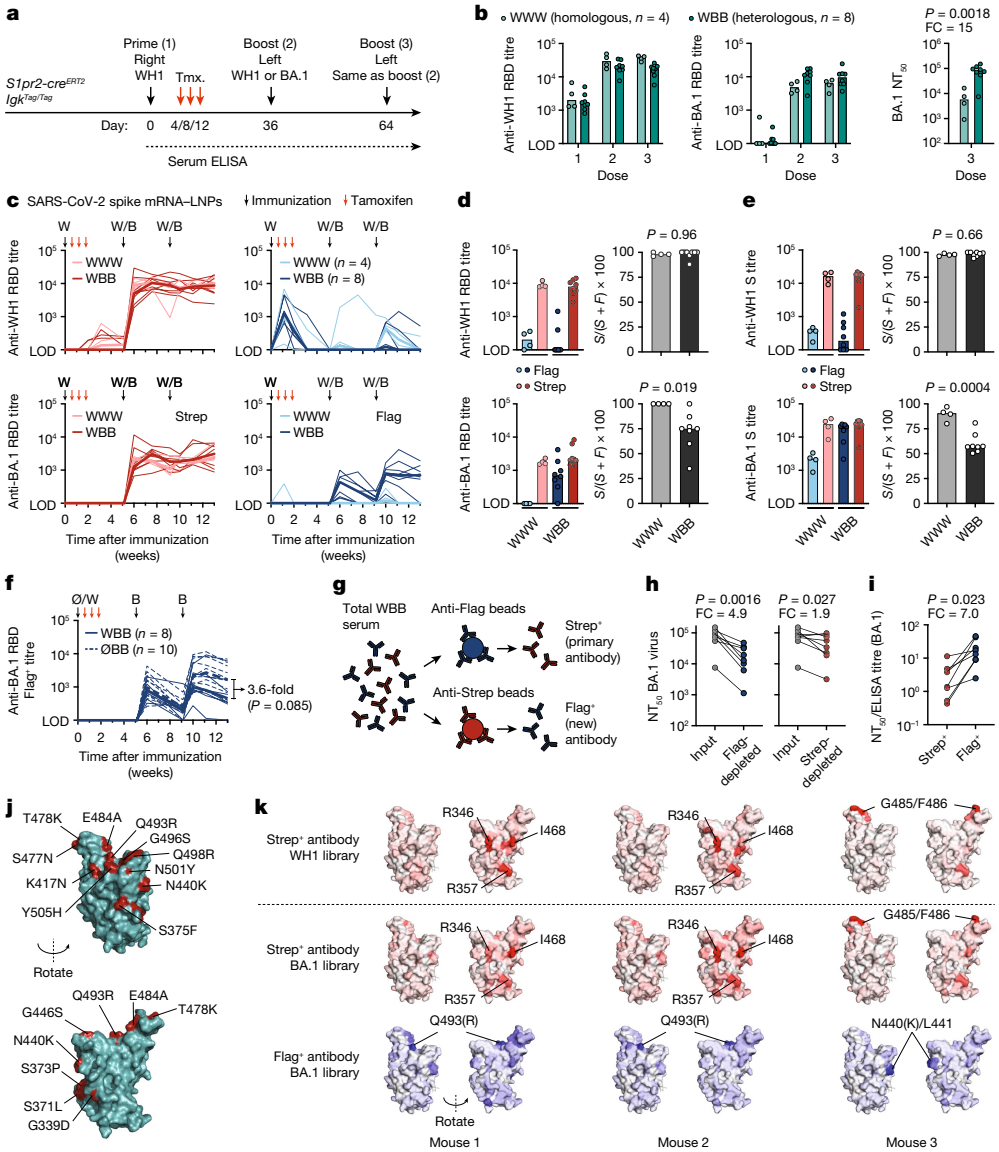

Fig. 4 | Subversion of primary addiction by heterologous SARS-CoV-2 boosting. a, Schematic of the immunization strategies. **b**, Anti-WH1 (left) and BA.1 RBD IgG titres (middle) and NT_{50} of BA.1 pseudovirus (right) 2 weeks after the indicated dose in homologously (WWW) or heterologously (WBB) immunized *S1pr2-Igk*$^{Tag/Tag}$ mice. *P* values were calculated using two-tailed *t*-tests. FC, fold change. **c**, Evolution of anti-WH1 and BA.1 RBD tag-specific titres. The thin lines represent individual mice and the thick lines link the medians of log-transformed titre values. **d**, Comparison of the Flag and Strep anti-RBD titres shown in **c** at 2 weeks after the third immunization (left) along with primary addiction index (right). *P* values were calculated using two-tailed *t*-tests. **e**, Anti-full-S tag-specific titres and the primary addiction index for the same samples as in **d**, 2 weeks after the third dose. The results in **b**–**d** are from two independent experiments; the number of mice in each group is indicated. **f**, Comparison of de novo Flag$^+$ antibody responses in WBB mice versus mice in which the first dose and fate-mapping were omitted (ØBB). ØBB data are for ten mice from two independent experiments. WBB data are from **c**, remeasured in the same assay as ØBB. **g**, Schematic of antibody fractionation for the neutralization assay. **h**, BA.1 NT_{50} titres for WBB mice at the same timepoint as in **d**. Post-depletion NT_{50} values were normalized as described in the Methods. *P* values were calculated using one-tailed paired *t*-tests. **i**, The potency of the anti-RBD BA.1 Strep$^+$ (Flag-depleted) and Flag$^+$ (Strep-depleted) fractions. Raw NT_{50} values for each fraction were divided by their respective RBD ELISA titres. *P* values were calculated using two-tailed paired *t*-tests. **j**, WH1 RBD structure (PDB: 6M0J) with amino acid changes in BA.1 highlighted in red. **k**, Deep mutational scanning analysis of serum samples obtained from three WBB mice 2 weeks after third immunization as in **d**. Antibody-binding sites on RBD are shaded according to escape fraction. The positions that are most highly targeted by each serum fraction are indicated (BA.1-specific residues are shown in parentheses).

WH1 immunization (ØBB) generated responses that were only 3.6-fold higher than the WBB (WH1-BA.1-BA.1) group (a difference that did not reach statistical significance; Fig. 4f), again showing that the effect of primary addiction in this setting is greatly reduced compared with that observed for homologous boosting (Fig. 2g). We conclude that BA.1 is sufficiently divergent from WH1 to induce substantial de novo antibody responses, even if it is not able to entirely overcome primary addiction. Moreover, the key difference between boosting homologously and heterologously is that only the latter can elicit a robust de novo response to the drifted strain.

To determine whether the enhanced neutralization of BA.1 observed after heterologous boosting (Fig. 4b) was due to the induction of new BA.1-specific antibodies in this setting, we fractionated WBB serum samples taken 2 weeks after the third immunization into Flag-depleted

(Strep$^+$, primary) and Strep-depleted (Flag$^+$, new) preparations (Fig. 4g and Extended Data Fig. 5a) and measured their neutralizing potency against WH1 and BA.1 pseudovirus. As expected, depletion of Flag$^+$ antibodies had minimal effect on WH1 neutralization, whereas Strep$^+$ depletion resulted in a much greater decrease (1.7-fold versus 8.5-fold, respectively; Extended Data Fig. 5b,c). By contrast, removing new (Flag$^+$) antibodies from WBB sera resulted in a greater reduction in BA.1 neutralization compared with removing primary (Strep$^+$) antibodies (4.9-fold versus 1.9-fold decrease; Fig. 4h), even though Strep$^+$ antibodies bound more avidly to the BA.1 RBD by ELISA (Fig. 4d). To estimate the neutralizing potency per unit of specific antibody, we divided the 50% neutralization titre (NT_{50}) derived from the BA.1 pseudovirus assay by the end-point binding titre obtained by BA.1 RBD-specific ELISA. When normalized to reactivity in this manner, new (Flag$^+$) antibody was on average 7.0-fold more potent at neutralizing BA.1 than the Strep$^+$ antibody produced by primary-cohort B cell clones in response to WH1 (Fig. 4i). As calculated in Extended Data Fig. 5d, around 80% of the excess BA.1 neutralization by WBB compared with WWW samples could be attributed to de novo generation of BA.1-specific antibodies from naive cells rather than to secondary affinity maturation or preferential selection of primary-cohort memory B cells. Thus, the antibodies that escape primary addiction after BA.1 boosting are optimized to neutralize the variant strain.

Finally, to gain mechanistic insights into how antigenic drift leads to attenuation of primary addiction, we performed deep mutational scanning[31,32] to define the WH1 and BA.1 RBD epitopes targeted by Flag$^+$ and Strep$^+$ antibodies in heterologously boosted mice (Fig. 4j and Extended Data Fig. 6). This approach enabled us to separately determine the epitopes targeted by primary and new antibody in the same mouse. We measured the antibody escape patterns of four mice against BA.1 (both Strep$^+$ and Flag$^+$ antibodies) and WH1 RBD (Strep$^+$ antibodies only), three of which showed interpretable dominance peaks (Extended Data Fig. 7). In these three mice, there was clear segregation of the epitopes targeted by primary Strep$^+$ and new Flag$^+$ antibodies (Fig. 4k and Extended Data Fig. 7). In two mice, Strep$^+$ antibodies targeted residues of the 'class 3' epitope located on the outer face of the RBD (Arg346, Arg357, Ile468), which, as expected, were conserved between WH1 and BA.1 (Fig. 4j,k). By contrast, Flag$^+$ antibodies in both mice were focused on the BA.1-specific residue Arg493 (Gln493 in WH1), located on the top of the RBD in the 'class 2' region of the ACE2-binding surface. The third mouse showed analogous segregation between primary and new antibodies but targeted to different epitopes. Whereas Strep$^+$ antibodies were heavily focused on the conserved class 1/2 epitope that includes Gly485/Phe486 (on the top of the RBD at the ACE2 interface), Flag$^+$ antibodies bound primarily to an epitope that includes the BA.1-specific Lys440 residue (Asn440 in WH1) on the side face of the RBD distal to Gly485/Phe486 (class 3). Notably, both N440K and Q493R have been reported to lead to escape from neutralization by various monoclonal antibodies[33–35]. Thus, all three mice followed a logic in which new antibodies elicited by heterologous immunization preferentially targeted epitopes that contained BA.1-specific escape mutations and that did not overlap with epitopes bound by cross-reactive primary antibodies. We conclude that primary addiction, by acting in an epitope-specific manner, suppresses the de novo generation of antibodies to conserved epitopes, while allowing the induction of new antibodies targeted specifically to drifted epitopes.

Discussion

Taken together, on the basis of our findings using the K-tag system, we make two main points. First, suppression of de novo antibody responses by existing immunity, a necessary feature of OAS as we define it, is extremely potent when measured at zero antigenic distance. These findings support the primary addiction/OAS[2] model (Fig. 2a) in which existing responses prevent the emergence of new serum antibodies to the same antigen, over a sequential contribution/seniority[20] model in which first-cohort responses are larger simply because they were established first and therefore boosted a greater number of times. Second, primary addiction weakens markedly as antigenic distance between priming and boosting strains increases. This observation suggests an explanation for why OAS has been so difficult to document experimentally in a consistent manner[5]—traditional measurements, which rely on differences between drifted antigens to assign antibodies to primary or de novo cohorts, may be able to distinguish these cohorts reliably only when antigenic distance is too great to allow for clear detection of primary addiction. A case in point is that our model estimates that primary addiction between PR8 and FM1, the influenza virus strains for which OAS was initially described[1,19], is relatively weak (equivalent to a 3.8-fold suppression of the de novo response), and may therefore be difficult to ascertain without the precision afforded by the K-tag model.

Our data are consistent with observations in humans showing that, after seasonal influenza vaccination, a large proportion of serum antibody clonotypes are recalled from pre-existing pools, although these studies remained agnostic to whether vaccine-induced antibody clonotypes arose from de novo responses or from recall of undetected memory B cells[17,36]. Humans, even with their rich influenza antigen exposure history, are able to mount substantial de novo responses in recall GCs, while relying on memory B cells for the immediate plasma cell response[37]. We therefore expect the general mechanics of primary addiction reported here to apply to humans as well, at least in general terms. In the SARS-CoV-2 setting, OAS-type suppression may explain the small and variable differences in the preferential induction of Omicron neutralization by variant-specific or bivalent compared with homologous vaccination[38–42]. Our data suggest that a second dose of an Omicron-containing vaccine may be required to reveal the full extent of de novo antibody induction by Omicron boosting. However, in practice, the repeated exposure of most individuals to WH1 antigens before Omicron boosting, as well as the potential greater propensity of human GCs to allow entry of reactivated memory B cells[37], may lead to stronger OAS-type suppression of Omicron-specific antibodies in real-life scenarios.

Mechanistically, our measurements at zero antigenic distance indicate a functional divide between recall GCs and serum responses in mice—whereas the former consist almost exclusively of naive-derived B cell clones[21–23], the latter are dominated by the effects of primary addiction. A potential explanation for this divergence is that the naive B cells that contribute to secondary GCs are not of sufficient affinity either to exit the GC as plasma cells or to secrete antibodies that are detectable by direct ELISA. Low antigen binding among naive-derived secondary GC B cells has been reported previously by others[22], which is consistent with the latter hypothesis. As antigenic drift for both influenza virus and SARS-CoV-2 is primarily driven by immune escape, the loosening of OAS in heterologous settings should in principle focus newly recruited B cell clones on drifted neutralizing epitopes. This view is supported by the results of our neutralization and epitope mapping experiments. Moreover, RBD-binding antibodies that escaped primary addiction tended to focus on new residues located within epitopes that were not dominant targets of the cross-reactive first-cohort response. This pattern suggests antibody-mediated epitope masking—whereby serum antibodies that are either present before boosting or produced acutely by boosted memory B cells compete with naive B cells for binding to a specific epitope—as a potential mechanism for primary addiction. Similar effects have been observed previously by infusion of monoclonal antibodies before induction of an immune response in mice and humans and are predicted to affect the fine specificity of recall responses[43–46]. These findings not only indicate that the suppression of de novo antibody responses afforded by primary addiction is epitope specific rather than antigen specific (epitope masking, rather than antigen trapping[47]), but also suggest a teleological explanation for why it might be advantageous for memory B cells to avoid re-entering

secondary GCs[21,48], as competition by memory B cells could inhibit the ability of naive cells to generate antibodies tailored to new epitopes in viral escape variants. In such a framework, the primary role of secondary GCs would be to circumvent the worst effects of OAS.

Online content

Any methods, additional references, Nature Portfolio reporting summaries, source data, extended data, supplementary information, acknowledgements, peer review information; details of author contributions and competing interests; and statements of data and code availability are available at https://doi.org/10.1038/s41586-023-05715-3.

1. Francis, T. On the doctrine of original antigenic sin. *Proc. Am. Phil. Soc.* **104**, 572–578 (1960).
2. Fazekas de St Groth, S. & Webster, R. G. Disquisitions on original antigenic sin. II. Proof in lower creatures. *J. Exp. Med.* **124**, 347–361 (1966).
3. Cobey, S. & Hensley, S. E. Immune history and influenza virus susceptibility. *Curr. Opin. Virol.* **22**, 105–111 (2017).
4. Henry, C., Palm, A. E., Krammer, F. & Wilson, P. C. From original antigenic sin to the universal influenza virus vaccine. *Trends Immunol.* **39**, 70–79 (2018).
5. Yewdell, J. W. & Santos, J. J. S. Original antigenic sin: how original? How sinful? *Cold Spring Harb. Perspect. Med.* **11**, a038786 (2021).
6. Krammer, F. The human antibody response to influenza A virus infection and vaccination. *Nat. Rev. Immunol.* **19**, 383–397 (2019).
7. Wheatley, A. K. et al. Immune imprinting and SARS-CoV-2 vaccine design. *Trends Immunol.* **42**, 956–959 (2021).
8. Monto, A. S., Malosh, R. E., Petrie, J. G. & Martin, E. T. The doctrine of original antigenic sin: separating good from evil. *J. Infect. Dis.* **215**, 1782–1788 (2017).
9. Victora, G. D. & Nussenzweig, M. C. Germinal centers. *Annu. Rev. Immunol.* **40**, 413–442 (2022).
10. Baumgarth, N. The shaping of a B cell pool maximally responsive to infections. *Annu. Rev. Immunol.* **39**, 103–129 (2021).
11. Bhattacharya, D. Instructing durable humoral immunity for COVID-19 and other vaccinable diseases. *Immunity* **55**, 945–964 (2022).
12. Pulendran, B. & Ahmed, R. Immunological mechanisms of vaccination. *Nat. Immunol.* **12**, 509–517 (2011).
13. Gaebler, C. et al. Evolution of antibody immunity to SARS-CoV-2. *Nature* **591**, 639–644 (2021).
14. Tan, J. et al. A LAIR1 insertion generates broadly reactive antibodies against malaria variant antigens. *Nature* **529**, 105–109 (2016).
15. Davis, C. W. et al. Longitudinal analysis of the human B cell response to ebola virus infection. *Cell* **177**, 1566–1582 (2019).
16. Turner, J. S. et al. SARS-CoV-2 mRNA vaccines induce persistent human germinal centre responses. *Nature* **596**, 109–113 (2021).
17. Lee, J. et al. Molecular-level analysis of the serum antibody repertoire in young adults before and after seasonal influenza vaccination. *Nat. Med.* **22**, 1456–1464 (2016).
18. Han, J. et al. Polyclonal epitope mapping reveals temporal dynamics and diversity of human antibody responses to H5N1 vaccination. *Cell Rep.* **34**, 108682 (2021).
19. Francis, T. Jr. Influenza: the new acquayantance. *Ann. Intern. Med.* **39**, 203–221 (1953).
20. Lessler, J. et al. Evidence for antigenic seniority in influenza A (H3N2) antibody responses in southern China. *PLoS Pathog.* **8**, e1002802 (2012).
21. Mesin, L. et al. Restricted clonality and limited germinal center reentry characterize memory B cell reactivation by boosting. *Cell* **180**, 92–106 (2020).
22. Viant, C. et al. Antibody affinity shapes the choice between memory and germinal center B cell fates. *Cell* **183**, 1298–1311 (2020).
23. Kuraoka, M. et al. Recall of B cell memory depends on relative locations of prime and boost immunization. *Sci. Immunol.* **7**, eabn5311 (2022).
24. Mostoslavsky, R., Alt, F. W. & Rajewsky, K. The lingering enigma of the allelic exclusion mechanism. *Cell* **118**, 539–544 (2004).
25. Shinnakasu, R. et al. Regulated selection of germinal-center cells into the memory B cell compartment. *Nat. Immunol.* **17**, 861–869 (2016).
26. Smith, D. J., Forrest, S., Ackley, D. H. & Perelson, A. S. Variable efficacy of repeated annual influenza vaccination. *Proc. Natl Acad. Sci. USA* **96**, 14001–14006 (1999).
27. Fonville, J. M. et al. Antibody landscapes after influenza virus infection or vaccination. *Science* **346**, 996–1000 (2014).
28. Hogan, M. J. & Pardi, N. mRNA vaccines in the COVID-19 pandemic and beyond. *Annu. Rev. Med.* **73**, 17–39 (2022).
29. Schmidt, F. et al. Measuring SARS-CoV-2 neutralizing antibody activity using pseudotyped and chimeric viruses. *J. Exp. Med.* **217**, e20201181 (2020).
30. Muecksch, F. et al. Affinity maturation of SARS-CoV-2 neutralizing antibodies confers potency, breadth, and resilience to viral escape mutations. *Immunity* **54**, 1853–1868.e7 (2021).
31. Greaney, A. J. et al. Comprehensive mapping of mutations in the SARS-CoV-2 receptor-binding domain that affect recognition by polyclonal human plasma antibodies. *Cell Host Microbe* **29**, 463–476 (2021).
32. Starr, T. N. et al. Prospective mapping of viral mutations that escape antibodies used to treat COVID-19. *Science* **371**, 850–854 (2021).
33. Liu, L. et al. Striking antibody evasion manifested by the Omicron variant of SARS-CoV-2. *Nature* **602**, 676–681 (2022).
34. McCallum, M. et al. Structural basis of SARS-CoV-2 Omicron immune evasion and receptor engagement. *Science* **375**, 864–868 (2022).
35. Weisblum, Y. et al. Escape from neutralizing antibodies by SARS-CoV-2 spike protein variants. *eLife* **9**, e61312 (2020).
36. Lee, J. et al. Persistent antibody clonotypes dominate the serum response to influenza over multiple years and repeated vaccinations. *Cell Host Microbe* **25**, 367–376 (2019).
37. Turner, J. S. et al. Human germinal centres engage memory and naive B cells after influenza vaccination. *Nature* **586**, 127–132 (2020).
38. Alsoussi, W. B. et al. SARS-CoV-2 Omicron boosting induces de novo B cell response in humans. Preprint at *bioRxiv* https://doi.org/10.1101/2022.09.22.509040 (2022).
39. Collier, A. Y. et al. Immunogenicity of BA.5 bivalent mRNA vaccine boosters. *N. Engl. J. Med.* https://doi.org/10.1056/NEJMc2213948 (2023).
40. Wang, Q. et al. Antibody response to Omicron BA.4–BA.5 bivalent booster. *N. Engl. J. Med.* https://doi.org/10.1056/NEJMc2213907 (2023).
41. Davis-Gardner, M. E. et al. Neutralization against BA.2.75.2, BQ.1.1, and XBB from mRNA bivalent booster. *N. Engl. J. Med.* **388**, 183–185 (2023).
42. Kurhade, C. et al. Low neutralization of SARS-CoV-2 Omicron BA.2.75.2, BQ.1.1 and XBB.1 by parental mRNA vaccine or a BA.5 bivalent booster. *Nat. Med.* https://doi.org/10.1038/s41591-022-02162-x (2022).
43. McNamara, H. A. et al. Antibody feedback limits the expansion of B cell responses to malaria vaccination but drives diversification of the humoral response. *Cell Host Microbe* **28**, 572–585 (2020).
44. Meyer-Hermann, M. Injection of antibodies against immunodominant epitopes tunes germinal centers to generate broadly neutralizing antibodies. *Cell Rep.* **29**, 1066–1073 (2019).
45. Tas, J. M. J. et al. Antibodies from primary humoral responses modulate recruitment of naive B cells during secondary responses. *Immunity* **55**, 1856–1871 (2022).
46. Schaefer-Babajew, D. et al. Antibody feedback regulates immune memory after SARS-CoV-2 mRNA vaccination. *Nature* **613**, 735–742 (2023).
47. Kok, A., Fouchier, R. A. M. & Richard, M. Cross-reactivity conferred by homologous and heterologous prime-boost A/H5 influenza vaccination strategies in humans: a literature review. *Vaccines* **9**, 1465 (2021).
48. Pape, K. A., Taylor, J. J., Maul, R. W., Gearhart, P. J. & Jenkins, M. K. Different B cell populations mediate early and late memory during an endogenous immune response. *Science* **331**, 1203–1207 (2011).

Methods

Mice

WT C57BL/6J and *B6.C(Cg)-Cd79a*$^{tm1(cre)Reth}$*/EhobJ* (*Cd79a*$^{Cre/+}$, also known as Mb1-Cre[49]) mice were obtained from The Jackson Laboratory. *S1pr2-cre*^{ERT2} BAC-transgenic mice[25] were a gift from T. Kurosaki and T. Okada. *Igk*^{Tag} mice were generated at the Rockefeller University. We designed the allele as indicated in Fig. 1a and Extended Data Fig. 1, with a Flag tag (DYKDDDDK) and Strep-II tag (WSHPQFEK) separated by stop codons and the SV40 poly-A transcriptional terminator. The 522-nucleotide single-stranded DNA template (including 5′ and 3′ homology arms, each 100 nucleotides long) and the CRISPR guide-RNA (GGAGCTGGTGGTGGCGTCTC) were purchased from IDT and prepared according to the Easi-CRISPR gene targeting method[50] by the Rockefeller University Gene Targeting Resource Center and injected into zygotes obtained from C57BL/6 mice by the Rockefeller University Transgenic Services core facility. We verified that the allele was correctly inserted by Sanger sequencing across the entire locus using genomic primers located outside of the homology arms. To decrease the risk of potential CRISPR off-target effects, one founder mouse was back-crossed for at least five generations onto C57BL/6J mice before use in experiments. To generate *Igk*$^{Flag/Strep}$ mice, germline-excised (Cre-negative mice displaying Strep$^+$ B cell surface staining) mice, obtained from occasional spontaneous germline recombination in *Cd79a*$^{Cre/+}$*Igk*^{Tag} breedings, were crossed to the parental *Igk*^{Tag} strain. All of the mice were held at the immunocore clean facility at the Rockefeller University under specific-pathogen-free conditions. All mouse procedures were approved by the Rockefeller University's Institutional Animal Care and Use Committee.

Immunizations, infections and treatments

Immune responses were induced in mice (male and female, aged 7–12 weeks) by either subcutaneous footpad immunization with 10 μg TNP_{17}-KLH (Biosearch, T-5060) supplemented with 1/3 volume of Imject alum (Thermo Fisher Scientific) or i.p. immunization with 50 μg TNP-KLH prepared with 1/3 volume of either alum or aluminium hydroxide gel (alhydrogel, Invivogen); 20 μg recombinantly produced trimer-stabilized HA (see below) in alhydrogel; intramuscular immunization of quadricep muscles with 3 μg WH1 (ref. [51]) or BA.1 spike mRNA encapsulated in lipid nanoparticles (mRNA–LNP), generated as described below; or by intranasal infection with mouse-adapted PR8 influenza virus produced in embryonated chicken eggs (~33 plaque-forming units, provided by M. Carroll). In *S1pr2-Igk*^{Tag} mice, the primary immune response was fate-mapped by oral gavage of 200 μl tamoxifen (Sigma-Aldrich) dissolved in corn oil at 50 mg ml^{-1}, on days 4 and 8 for the day 12 flow cytometry experiment (Fig. 1), on days 4, 8 and 12 for all other immunization experiments, and on days 4, 8, 12 and 16 for the influenza infection experiment (Fig. 3). In TNP recall experiments (Fig. 2c), boosting was performed identically to the primary immunization, at the indicated time points. For homologous mRNA–LNP experiments (Fig. 2e), boosting was performed in the same way as priming, except that, for some mice, the left quadricep muscle was boosted (contralaterally, stratified in Extended Data Fig. 3e). For heterologous mRNA–LNP recall experiments (Fig. 4), boosting was contralateral in all cases. For HA immunization experiments (Fig. 3), homologous or heterologous HA protein boosting was performed ipsilaterally, exactly as the primary immunization. For infection experiments, mice were boosted after 3 months by subcutaneous immunization of the footpad with 5 μg HA_{PR8} or HA_{FM1} prepared with 1/3 volume alhydrogel, as described previously[21]. In all cases, additional booster immunizations were performed identically to the first boost. Blood samples were collected by cheek puncture into microtubes prepared with clotting activator serum gel (Sarstedt, 41.1378.005).

Generation of recombinant and hapten-conjugated proteins

Recombinant HAs used for immunizations and ELISAs were produced in-house using the CHO cell protein expression system, as described previouosly[21]. Cysteine residues were introduced into the HA sequence to create trimer-stabilizing disulfide bonds, as originally described for H1/A/California/07/2009 (ref. [52]). We described the production of HA_{PR8} and HA_{CA09} previously[21]. For HA_{FM1} and HA_{NC99}, the same procedure was followed, including the introduction of trimer-stabilizing mutations. For immunizations, C-terminal domains not native to HA (foldon, Avi-tag, His-tag) were removed by thrombin cleavage and HAs were subsequently fast protein liquid chromatography (FPLC)-purified before storage in phosphate-buffered saline (PBS). For ELISA, non-thrombin treated FPLC-purified proteins were used. A high-affinity IgY-specific monoclonal antibody obtained from CGG-immunized mice (clone 2.1 (ref. [53])) was modified for use as a standard for Flag/Strep ELISA detection. Heavy and light chain constant regions in the original human monoclonal antibody plasmids[54] were replaced with the mouse IgG_1 and Igκ constant regions and the C terminus of $C_κ$ was modified to encode a LoxP site and a Ser-Gly-Gly linker followed by either a Flag or Strep-tag, yielding $C_κ$ chains that were identical to those produced by *Igk*^{Tag} mice before and after recombination, respectively. The mAb-Flag or mAb-Strep light-chain plasmids were transfected together with the heavy chain plasmid into HEK293F cells (Thermo Fisher Scientific, R79007) and purified using protein-G affinity chromatography as described previously[53]. Cell lines tested negative for mycoplasma and were not authenticated besides testing the protein they produced. To compare affinity maturation between Flag$^+$ and Strep$^+$ anti-TNP antibody titres (Fig. 1h), custom low- and high-hapten bovine serum albumin (BSA) conjugations were made in-house. BSA (in PBS; Thermo Fisher Scientific, 77110) at 2.5 mg ml^{-1} was incubated with TNP-ε-aminocaproyl-OSu (Biosearch Technologies, T-1030) in PBS with 20% dimethyl sulfoxide at a molar ratio of either 1:2 or 1:20 for 2 h at room temperature while rotating. Unconjugated TNP-ε-Aminocaproyl-OSu was removed by dialysis in PBS. Final TNP:BSA conjugation ratios were estimated to be ~1:1 and ~1:13 by measuring absorbance at 280 and 348 nm, these reagents are referred to as TNP_1-BSA and TNP_{13}-BSA. The BSA concentration was corrected by determining the extinction coefficient for TNP-ε-aminocaproyl-OSu at 280 nm. Except for in Fig. 1h, commercial TNP_4-BSA (Biosearch Technologies, T-5050) was used for all other TNP ELISAs (described below).

Production of mRNA–LNP

The WH1 S mRNA vaccine was designed on the basis of the SARS-CoV-2 S protein sequence (Wuhan-Hu-1, GenBank: MN908947.3) where the lysine and valine amino acids in positions 986–987 were modified to proline residues to obtain a prefusion-stabilized mRNA-encoded immunogen. The BA.1 S amino acid sequence was obtained from the WH1 S by introducing BA.1-specific modifications. Coding sequences of the WH1 and BA.1 S were codon-optimized, synthesized and cloned into an mRNA production plasmid (GenScript) as described previously[55]. mRNA production and LNP encapsulation was performed as described previously[55]. In brief, mRNAs were transcribed to contain 101 nucleotide-long poly(A) tails. m1Ψ-5′-triphosphate (TriLink) instead of UTP was used to generate modified nucleoside-containing mRNAs. Capping of the in vitro transcribed mRNAs was performed co-transcriptionally using the trinucleotide cap1 analogue, CleanCap (TriLink). mRNA was purified by cellulose (Sigma-Aldrich) purification, as described previously[56]. All mRNAs were analysed by agarose gel electrophoresis and were stored frozen at −20 °C. Cellulose-purified m1Ψ-containing RNAs were encapsulated in LNPs using a self-assembly process as previously described, whereby an ethanolic lipid mixture of ionizable cationic lipid, phosphatidylcholine, cholesterol and polyethylene glycol-lipid was rapidly mixed with an aqueous solution containing mRNA at acidic pH[57]. The ionizable cationic lipid and LNP composition are described in the patent application WO 2017/004143. The RNA-loaded particles were characterized and subsequently stored at −80 °C at a concentration of 1 μg μl^{-1}. The mean hydrodynamic diameter of these mRNA–LNPs was around

80 nm with a polydispersity index of 0.02–0.06 and an encapsulation efficiency of approximately 95%.

Flow cytometry

For flow cytometry analysis of peripheral B cells, blood was collected in microtubes with ethylenediaminetetraacetic acid (EDTA) to prevent coagulation and treated with ammonium–chloride–potassium (ACK) buffer (Lonza) to lyse red blood cells. For lymph node samples, cell suspensions were obtained by mechanical disassociation with disposable micropestles (Axygen). Spleens were homogenized by filtering through a 70 µm cell strainer and treated with ACK buffer. Bone marrow cells were extracted by centrifugation of punctured tibiae and femurs at up to 10,000*g* for 10 s, then treated with ACK buffer. Cells from each tissue were resuspended in PBS supplemented with 0.5% BSA and 1 mM EDTA and incubated first with FC-block (rat anti-mouse CD16/32, 2.4G2, Bio X Cell) for 30 min on ice and subsequently with various fluorescently labelled antibodies (Supplementary Table 1) for 30 min. Cells were filtered and washed with the same buffer before analysis on a BD FACS Symphony cytometer. Data were analysed using FlowJo (v.10).

Western blotting

To determine the presence of epitope-tagged antibodies in *Igk*^{Tag} mice, serum samples from steady state adult mice and precision plus dual-colour protein standards (Bio-Rad) were run in triplicate on SDS–PAGE mini-protean TGX protein gels (Bio-Rad) under denaturing conditions, to separate heavy and light antibody chains. The samples were transferred to a polyvinylidene difluoride membrane using the Iblot gel transfer system (Invitrogen). Membranes were blocked for 2 h at room temperature while gently shaking with 5% non-fat dry milk in PBS-Tween-20 (0.05%), before overnight incubation in the same buffer with 1:2,000 anti-Flag-HRP (D6W5B, Cell Signalling Technology, 86861S) or anti-Strep (Strep-tag II StrepMAB-Classic, Bio-Rad, MCA2489P) or goat anti-mouse Igκ-HRP (Southern Biotech, 1050-05). Membranes were extensively washed with PBS-Tween-20 and subsequently incubated with western blotting ECL substrate (Amersham) before chemiluminescence detection using the Azure c300 gel imager (Azure Biosystems).

ELISA

ELISAs were performed as described previously[21], with specific modifications to allow for direct Flag/Strep comparison. Flag/Strep ELISAs were performed side by side and with internal standards on each 96-well plate. To detect antigen-specific serum antibody titres, the plates were coated overnight at 4 °C with antigen in PBS (10 µg ml^{-1} for TNP_4-BSA, 2 µg ml^{-1} for in-house-conjugated $TNP_{1/13}$-BSA (see above), and 1 µg ml^{-1} for HAs and SARS-CoV-2 spike or RBD proteins (Sinobiological, 40592-V08H, 40592-V08H121, 40589-V08H26; WH1 S and RBD proteins were a gift from P. Wilson)). For Flag/Strep standard curves, wells were coated with 10 µg ml^{-1} purified IgY (Gallus Immunotech). After washing with PBS-Tween (PBS + 0.05% Tween-20, Sigma-Aldrich), plates were blocked for 2 h at room temperature with 2.5% BSA in PBS. Serum samples were diluted 1:100 in PBS and serially titrated in threefold dilutions. Mouse anti-IgY mAb-Flag or mAb-Strep were also serially titrated in threefold dilutions (Extended Data Fig. 2d). The samples were incubated for 2 h and then washed with PBS-Tween, before adding one of the following HRP-detection antibodies: goat anti-mouse IgG (Jackson Immunoresearch, 15-035-071), rat anti-mouse Igκ (Abcam, ab99632), goat anti-mouse IgM (Southern Biotech, 1020-05), rabbit anti-Flag-HRP (D6W5B) or mouse anti-Strep (Strep-tag II StrepMAB-Classic) for 30–45 min. Dilutions of anti-Flag and anti-Strep antibodies were defined so that the curves generated by titration of Flag- and Strep-tagged monoclonal antibodies were equivalent (Extended Data Fig. 2d). After washing with PBS-Tween, samples were incubated with 3,3′,5,5′-tetramethylbenzidine substrate (slow kinetic form, Sigma-Aldrich) and the reaction was stopped with 1 N HCl. Optical density (OD) absorbance was measured at 450 nm on the Fisher Scientific accuSkan FC plate reader. To normalize Flag and Strep end-point titres, the serum titre dilution was calculated at which each sample passed the threshold OD value of its respective monoclonal antibody at a fixed concentration of either 20 or 6.67 ng µl^{-1}. Titres were calculated by logarithmic interpolation of the dilutions with readings immediately above and immediately below the monoclonal antibody OD used[58].

For total serum IgG ELISAs, plates were coated with anti-mouse IgG. Standard curves were generated using unlabelled mouse IgG (Southern Biotech, 0107-01), and detection was performed using anti-mouse IgG-HRP (Southern Biotech). To deplete IgM from the serum samples, anti-mouse IgM agarose beads (Sigma-Aldrich, A4540) were used according to the manufacturer's instructions. Beads were washed with PBS and samples were incubated at a ratio of 1:20 sample to beads overnight at 4 °C with rotation. The bead-bound IgM fraction was removed by centrifugation for 3 min at 10,000*g*, and the unbound supernatant fraction was used for subsequent ELISAs. To confirm the efficiency of IgM depletion, total IgM levels were measured as described above for total IgG, with goat anti-mouse IgM, unlabelled IgM and anti-mouse IgM-HRP (Southern Biotech).

Serum fractionation and SARS-CoV-2 pseudoneutralization assay

Virus neutralization titres were assessed in the Flag$^+$ versus Strep$^+$ serum fractions of samples collected from S mRNA–LNP immunized *S1pr2-Igk*^{Tag} mice. To separate fractions, immunoprecipitation with anti-Flag M2 magnetic beads (Sigma-Aldrich, M8823-5ML) and MagStrep type 3 XT beads (IBA, 2-4090-010) was performed according to the manufacturer's instructions. In brief, magnetic beads were washed with sample buffer (Tris-buffered saline for Flag beads, and 1× buffer W (IBA, 2-1003-100) for MagStrep beads) and the samples were incubated at a ratio of 20:1 sample to bead resin overnight at 4 °C with rotation. Bead-bound fractions were separated using a magnetic separator and discarded, while the unbound fraction was collected. Fractionated samples were concentrated by centrifugation to half the input concentration and heat inactivated. The degree to which the total and fractionated serum samples neutralized WH1 and BA.1 SARS-CoV-2 was approximated using SARS-CoV-2 spike pseudotyped HIV-1 based NanoLuc luciferase reporter assay described previously[29]. In brief, serum samples were five-fold serially diluted with a final top dilution of 1:00 serum and incubated for 1 h at 37 °C with SARS-CoV-2 WH1 or BA.1 spike pseudotyped HIV-1 reporter virus and then transferred to HT1080/ACE2.cl14 cells[59]. At 48 h, the cells were washed and lysed and the luciferase activity was measured using the Nano-Glo Luciferase Assay System (Promega) and the Glomax Navigator luminometer (Promega). The relative luminescence units were normalized using cells infected in the absence of serum and then plotted in GraphPad Prism. NT_{50} values were calculated using four-parameter nonlinear regression (least squares regression method without weighting) of the curves shown in Extended Data Fig. 5b. The mean of two technical duplicates is shown, outlier points were excluded. For NT_{50} comparisons between the input and fractions (Fig. 4g and Extended Data Fig. 5c), the NT_{50} of the fractionated samples was adjusted to equalize the BA.1 RBD ELISA titre of the undepleted tag compared to its corresponding ELISA titre in the input fraction.

Deep mutational scanning

Construction of yeast-displayed deep mutational scanning libraries of Omicron BA.1 RBD. Duplicate single-mutant site-saturation variant libraries were designed in the background of the SARS-CoV-2 Omicron BA.1 spike RBD and produced by Twist Bioscience, essentially the same as has been done previously for other SARS-CoV-2 variants[60,61]. The GenBank map of the plasmid encoding the unmutated Omicron BA.1 RBD in the yeast-display vector is available at GitHub (https://github.com/jbloomlab/SARS-CoV-2-RBD_DMS_Omicron/blob/main/

data/3294_pETcon-SARS2-RBD_Omicron-BA1.gb). The site-saturation variant libraries were delivered as double-stranded DNA fragments by Twist Bioscience and were barcoded and cloned in bulk into the yeast-display vector backbone. The barcoded mutant library plasmid DNA was electroporated into *Escherichia coli* (NEB 10-beta electrocompetent cells, New England BioLabs, C3020K), and bottlenecked to around 1×10^5 CFU (an average of >25 barcodes per single mutant). Plasmid DNA was purified and transformed into the AWY101 yeast strain. Sixteen-nucleotide barcodes were associated with their BA.1 variants by PacBio sequencing, and the effects of mutations of RBD expression and ACE2 binding were measured, essentially as described[61]. These experiments are described and analysed at GitHub (https://github.com/jbloomlab/SARS-CoV-2-RBD_DMS_Omicron).

FACS sorting of yeast libraries to select mutations with reduced binding by polyclonal sera from immunized mice. Experiments mapping mutations that reduce RBD binding of sera from immunized mice were performed in biological duplicate with independent mutant WH1 or BA.1 RBD libraries, similarly to as previously described for monoclonal antibodies[62] and human polyclonal plasma samples[63]. First, 75 µl of each of the sera was twice-depleted of non-specific yeast-binding antibodies by incubating for 2 h at room temperature or overnight at 4 °C with 37.5 OD units of AWY101 yeast containing an empty vector, as described previously[63]. WH1 and BA.1 mutant RBD yeast libraries[61] were induced with galactose-containing, low-dextrose synthetic defined medium with casamino acids (SD-CAA, 6.7 g l^{-1} yeast nitrogen base, 5.0 g l^{-1} casamino acids, 1.065 g l^{-1} MES acid and 2% (w/v) galactose + 0.1% (w/v) dextrose) to express RBD, then washed and incubated with diluted serum for 1 h at room temperature with gentle agitation. Each tested combination of mouse serum against each WH1 or BA.1 RBD mutant library for loss of binding of Strep or Flag-tag antibodies was performed independently. For each serum, a subsaturating dilution was used such that the amount of fluorescent signal due to serum antibody binding to RBD was approximately equal across samples (1:1,000 for mapping of Strep antibodies against the WH1 libraries; 1:200 for mapping of Strep antibodies against the BA.1 libraries; and 1:50 for mapping of the Flag antibodies against the BA.1 libraries). The yeast libraries were then secondarily labelled for 1 h with 1:100 FITC-conjugated anti-MYC antibodies (Immunology Consultants Lab, CYMC-45F) to label for RBD expression and either 1:200 APC-conjugated Streptavidin (Invitrogen S-868) to label for bound Strep antibodies or APC-conjugated rat anti-Flag (BioLegend, 637308) to label for bound Flag-tagged antibodies. A flow cytometry selection gate was drawn to capture RBD mutants with reduced antibody binding for their degree of RBD expression. For each sample, around 4×10^6 cells were processed on the BD FACSAria II cell sorter. Serum-escaped cells were grown overnight in SD-CAA as defined above with 2% (w/v) dextrose, no galactose, and 100 U ml^{-1} penicillin + 100 µg ml^{-1} streptomycin to expand cells before plasmid extraction.

DNA extraction and Illumina sequencing. Plasmid DNA was extracted from 30 OD units (1.6×10^8 colony-forming units (CFU)) of preselection yeast populations and approximately 5 OD units (around 3.2×10^7 CFU) of overnight cultures of serum-escaped cells (Zymoprep Yeast Plasmid Miniprep II) as previously described[60,62]. The 16-nucleotide barcodes identifying each WH1 or BA.1 RBD variant were amplified by polymerase chain reaction and prepared for Illumina sequencing as described previously[60,62]. Barcodes were sequenced on the Illumina NextSeq 2000 system with 50 bp single-end reads.

Analysis of deep sequencing data to compute each mutation's escape fraction. Escape fractions were computed essentially as described previously[62]. We used the dms_variants package (https://jbloomlab.github.io/dms_variants/, v.1.4.0) to count each barcoded RBD variant in each preselection and serum-escape population. For each selection, we computed the escape fraction for each barcoded variant by the formula provided in ref. [62]. These escape fractions represent the estimated fraction of cells expressing that specific variant that falls in the escape bin, such that a value of 0 means the variant is always bound by serum and a value of 1 means that it always escapes serum binding. We then applied a computational filter to remove variants with >1 amino-acid mutation, low sequencing counts (<50 in the preselection condition) or highly deleterious mutations that might cause antibody escape simply by leading to poor expression of properly folded RBD on the yeast cell surface (an ACE2 binding score of <−2 or an RBD expression score of <−1.25 or <−0.83361 for the WH1 and BA.1 mutant libraries, respectively, reflecting the different baseline expression levels of the two wild-type RBDs). The reported antibody-escape scores throughout the paper are the average across duplicate libraries; these scores are also in Supplementary Table 1. Correlations in final single-mutant escape scores are shown in Extended Data Fig. 6c. Full documentation of the computational analysis is available at GitHub (https://github.com/jbloomlab/SARS-CoV-2-RBD_MAP_OAS).

Data visualization. The serum-escape map logo and line plots were created using the dmslogo package (https://jbloomlab.github.io/dmslogo, v.0.6.2). The height of each letter indicates the escape fraction for that amino-acid mutation. For each serum, the logo plots feature any site where for ≥1 library/antibody tag condition, the site-total antibody escape was >10× the median across all sites and at least 10% the maximum of any site. For each sample, the *y* axis was scaled to be the greatest of (1) the maximum site-wise escape metric observed for that sample or (2) 20× the median site-wise escape fraction observed across all sites for that plasma. The code that generates these logo plot visualizations is available at GitHub (https://github.com/jbloomlab/SARS-CoV-2-RBD_MAP_OAS/blob/main/results/summary/escape_profiles.md). To visualize serum escape on the RBD structure, the WH1 RBD surface (PDB: 6M0J) was coloured by the site-wise escape metric at each site, with white indicating no escape and red indicating the site with the most escape.

Statistical analysis and software

Statistical tests used to compare conditions are indicated in figure legends. No statistical methods were used to determine the sample size. Statistical analysis was carried out using GraphPad Prism v.9. Flow cytometry analysis was carried out using FlowJo (v.10). Graphs were plotted using Prism (v.9) and edited for appearance using Adobe Illustrator CS. For data plotted on logarithmic scales (such as serum antibody titres), statistical analysis was performed on the log-transformed data. Samples with reactivities below the limit of detection were assigned a value of 100, as the top dilution was 1:100.

Reporting summary

Further information on research design is available in the Nature Portfolio Reporting Summary linked to this article.

Data availability

The raw Illumina reads of the 16-nucleotide variant barcodes from the deep mutational scanning experiments are available at the NCBI SRA under BioProject PRJNA770094, BioSample SAMN30086726. All escape scores are shown in Supplementary Table 1 and are available at GitHub (https://github.com/jbloomlab/SARS-CoV-2-RBD_MAP_OAS/blob/main/results/supp_data/all_raw_data.csv). Renderings of spike RBD and HA structures were obtained from the PDB under accession codes 6M0J, 1RU7 and 3LZG.

Code availability

The full code used to analyse the deep mutational scanning experiments is available at GitHub (https://github.com/jbloomlab/

SARS-CoV-2-RBD_MAP_OAS). The code to generate the logo plot visualizations is available at GitHub (https://github.com/jbloomlab/SARS-CoV-2-RBD_MAP_OAS/blob/main/results/summary/escape_profiles.md).

49. Hobeika, E. et al. Testing gene function early in the B cell lineage in mb1-cre mice. *Proc. Natl Acad. Sci. USA* **103**, 13789–13794 (2006).
50. Quadros, R. M. et al. Easi-CRISPR: a robust method for one-step generation of mice carrying conditional and insertion alleles using long ssDNA donors and CRISPR ribonucleoproteins. *Genome Biol.* **18**, 92 (2017).
51. Laczko, D. et al. A single immunization with nucleoside-modified mRNA vaccines elicits strong cellular and humoral immune responses against SARS-CoV-2 in mice. *Immunity* **53**, 724–732 (2020).
52. Lee, P. S., Zhu, X., Yu, W. & Wilson, I. A. Design and structure of an engineered disulfide-stabilized influenza virus hemagglutinin trimer. *J. Virol.* **89**, 7417–7420 (2015).
53. Tas, J. M. et al. Visualizing antibody affinity maturation in germinal centers. *Science* **351**, 1048–1054 (2016).
54. Wardemann, H. et al. Predominant autoantibody production by early human B cell precursors. *Science* **301**, 1374–1377 (2003).
55. Freyn, A. W. et al. A multi-targeting, nucleoside-modified mRNA influenza virus vaccine provides broad protection in mice. *Mol. Ther.* **28**, 1569–1584 (2020).
56. Baiersdorfer, M. et al. A facile method for the removal of dsRNA contaminant from in vitro-transcribed mRNA. *Mol. Ther. Nucleic Acids* **15**, 26–35 (2019).
57. Maier, M. A. et al. Biodegradable lipids enabling rapidly eliminated lipid nanoparticles for systemic delivery of RNAi therapeutics. *Mol. Ther.* **21**, 1570–1578 (2013).
58. Ersching, J. et al. Germinal center selection and affinity maturation require dynamic regulation of mTORC1 kinase. *Immunity* **46**, 1045–1058 (2017).
59. Schmidt, F. et al. Plasma neutralization of the SARS-CoV-2 Omicron variant. *N. Engl. J. Med.* **386**, 599–601 (2022).
60. Starr, T. N. et al. Deep mutational scanning of SARS-CoV-2 receptor binding domain reveals constraints on folding and ACE2 binding. *Cell* **182**, 1295–1310 (2020).
61. Starr, T. N. et al. Shifting mutational constraints in the SARS-CoV-2 receptor-binding domain during viral evolution. *Science* **377**, 420–424 (2022).
62. Greaney, A. J. et al. Complete mapping of mutations to the SARS-CoV-2 spike receptor-binding domain that escape antibody recognition. *Cell Host Microbe* **29**, 44–57 (2021).
63. Greaney, A. J. et al. A SARS-CoV-2 variant elicits an antibody response with a shifted immunodominance hierarchy. *PLoS Pathog.* **18**, e1010248 (2022).

Acknowledgements We thank the staff at the Rockefeller University Transgenics and Gene Targeting facilities for generating the K-tag mouse strain and Comparative Biosciences Center for mouse housing; P. Wilson for recombinant SARS-CoV-2 WH1 spike and RBD protein; J. T. Jacobsen for technical assistance; and all of the Rockefeller University staff for their continuous support. This study was funded by NIH/NIAID grants R01AI119006 and R01AI139117 to G.D.V., P01AI165075 to P.D.B., R01AI146101 and R01AI153064 to N.P. and R01AI141707 to J.D.B. Work in the Victora laboratory is additionally supported by NIH grant DP1AI144248 (Pioneer award) and the Robertson Foundation. A.S. was supported by a Boehringer–Ingelheim Fonds PhD fellowship. P.D.B. and J.D.B. are HHMI investigators. G.D.V. is a Burroughs–Wellcome Investigator in the Pathogenesis of Infectious Disease, a Pew-Stewart Scholar and a MacArthur Fellow.

Author contributions A.S. and M.F.L.v.'t.W. performed all experimental work, with essential input from L.M. A.J.G. performed and interpreted the deep mutational scanning experiments under the supervision of T.N.S. and J.D.B. N.P. and H.M. designed and produced WH1 and BA.1 S-encoding mRNAs. P.J.C.L. and Y.K.T. formulated mRNAs into LNP. T.Z. carried out pseudovirus-neutralization assays under the supervision of P.D.B. A.S. and G.D.V. designed the K-tag allele and all of the experiments in the study and wrote the manuscript with input from all of the authors.

Competing interests N.P. is named on a patent (62/153,143 — Nucleoside-modified RNA inducing an adaptive immune response), describing the use of nucleoside-modified mRNA in LNPs as a vaccine platform. He has disclosed those interests fully to the University of Pennsylvania and has an approved plan in place for managing any potential conflicts arising from the licensing of that patent. P.J.C.L. and Y.K.T. are employees of Acuitas Therapeutics, a company that is involved in the development of mRNA–LNP therapeutics. Y.K.T. is named on a patent (WO 2017/004143 — Lipids and lipid nanoparticle formulations for delivery of nucleic acids) that describes LNPs for the delivery of nucleic acid therapeutics, including mRNA, and the use of modified mRNA in lipid nanoparticles as a vaccine platform. P.D.B. has done consulting work in the area of COVID vaccines for Pfizer. J.D.B. consults or has recently consulted for Apriori Bio, Oncorus, Merck and Moderna on topics related to viruses, vaccines and viral evolution. J.D.B, T.N.S. and A.J.G. are listed as inventors on Fred Hutch licensed patents (62/935,954 and 62/692,398) related to viral deep mutational scanning. G.D.V. and J.D.B. are advisors for the Vaccine Company.

Additional information

Supplementary information The online version contains supplementary material available at https://doi.org/10.1038/s41586-023-05715-3.

Correspondence and requests for materials should be addressed to Gabriel D. Victora.

Peer review information *Nature* thanks the anonymous reviewers for their contribution to the peer review of this work.

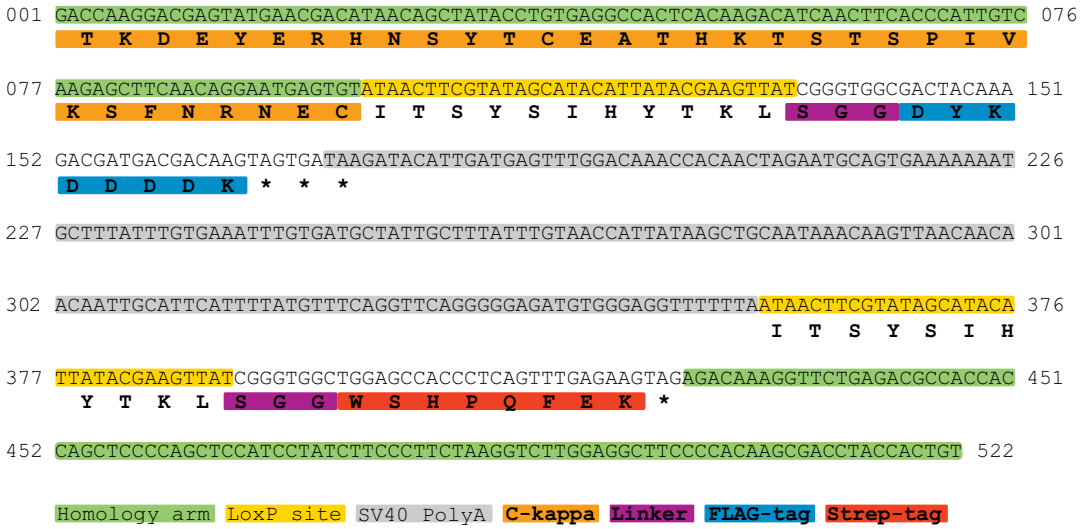

Extended Data Fig. 1 | Design of the K-tag allele. Nucleotide sequence of the 522 bp DNA template used to generate the *Igk*^{Tag} allele, with amino acid translations given for all coding sequences (bold font). Nucleotide numbers are given for each line. Amino acid translation is positioned below the centre nucleotide of each codon.

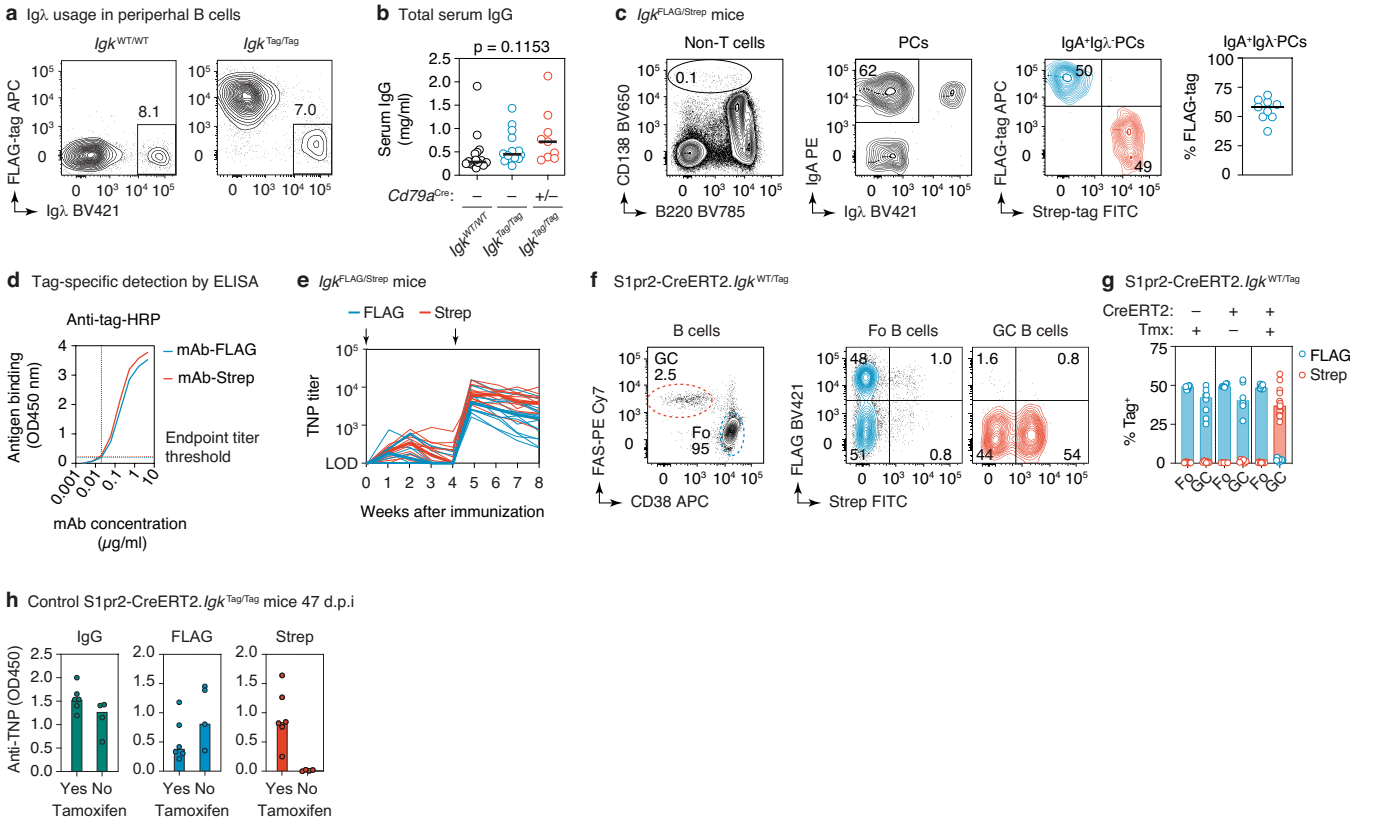

Extended Data Fig. 2 | Characterization of the K-tag system. (**a**) Representative flow cytometry plots of peripheral B cells (gated: $B220^+CD4^-CD8^-CD138^-$) obtained from the blood of WT and *Igk*$^{Tag/Tag}$ mice, stained for surface expression of Igλ and FLAG-tagged immunoglobulins. (**b**) Total IgG concentration in the serum of WT, *Igk*$^{Tag/Tag}$, and *Cd79a*$^{Cre/+}$.*Igk*$^{Tag/Tag}$ mice as determined by ELISA. Differences were not significant by one-way ANOVA ($p < 0.05$). (**c**) Flow cytometry of steady-state bone marrow plasma cells (PCs) obtained from adult (6-week old) *Igk*$^{FLAG/Strep}$ mice. Gating strategy for PCs is shown in the left panel (pre-gated on non-CD4/CD8 T cells), for surface IgA^+ and $Igλ^-$ PCs in the middle panel, and for FLAG/Strep in the right panel. Quantification across 9 mice from 3 independent experiments is shown in the rightmost panel (each dot represents an individual *Igk*$^{FLAG/Strep}$ mouse, line represents the median). (**d**) ELISA standard curves with monoclonal antibody (mAb)-FLAG and mAb-Strep detected at dilutions of the respective HRP antibodies where the curves overlap. The mAb concentration at which the curves crossed the absorbance background threshold (indicated by the dotted lines) was used to calculate the endpoint titre, as described in the methods section. (**e**) Tag-specific anti-TNP titres in *Igk*$^{FLAG/Strep}$ mice immunized and boosted i.p. with TNP-KLH/alum at the timepoints indicated by black arrows. Results are from 14 mice from 2 independent experiments. The day 7 timepoint was not collected for the first cohort. Thin lines represent individual mice, thick lines link medians of log transformed titre values at each time point. (**f**) Flow cytometry of S1pr2-*Igk*$^{WT/Tag}$ mice as in Fig. 1d,e. with quantification in (**g**), cre^- and no tamoxifen control groups are included. Data points are from 6–13 popliteal lymph nodes per group from at least 2 independent experiments. (**h**) Anti-TNP ELISA reactivity for S1pr2-*Igk*$^{Tag/Tag}$ mice immunized as in Fig. 1d. Serum was obtained at 47 d.p.i from 6 mice that received tamoxifen and 4 that did not receive tamoxifen. IgG (left), FLAG (middle) and Strep (right) ELISA absorbance is shown. Samples were diluted 1:100.

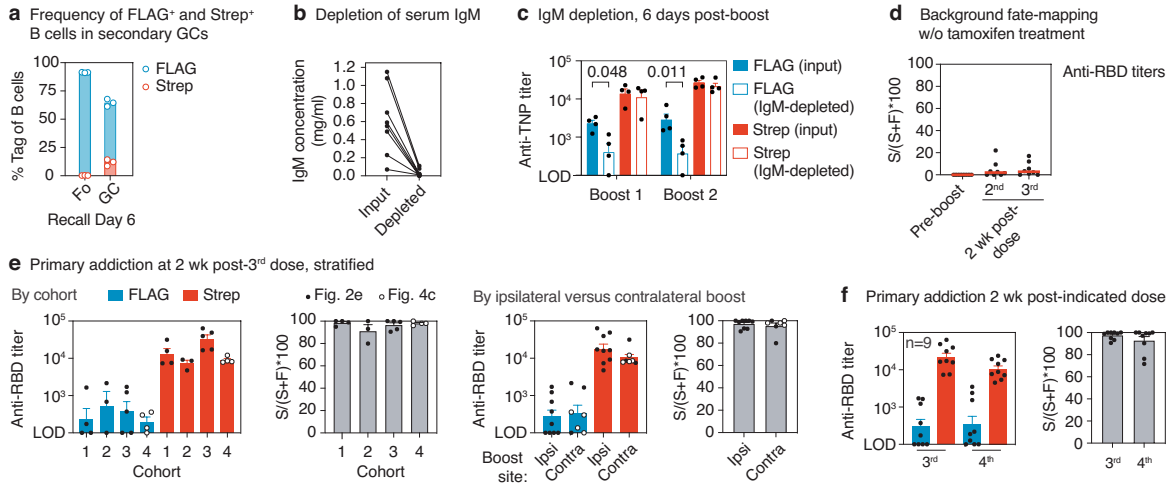

Extended Data Fig. 3 | Recall antibodies and GCs. (**a**) Flow cytometry of secondary GCs in the spleen of 3 TNP-KLH i.p. primed and boosted S1pr2-*Igk*$^{Tag/Tag}$ mice, with tamoxifen labelling at 4, 8, and 12 d.p.i.. Gated on GC B cells ($FAS^+CD38^-B220^+CD4^-CD8^-CD138^-$) expressing FLAG or Strep-tag as in Fig. 1e. (**b**) Total IgM concentrations of serum samples pre and post IgM-depletion via immunoprecipitation, measured by ELISA. Data are from 8 serum samples, from the same 4 mice as in Fig. 2c. (**c**) Tag-specific anti-TNP titres before and after IgM depletion for samples collected 6 days after the first and second boost with TNP-KLH (same samples as in (b) and Fig. 2c). Bars represent the means of log transformed titres and the error bars are SEM. P-values are for two-tailed, paired T-test, only statistically significant ($p < 0.05$) values are shown. (**d**) Background $Strep^+$ anti-RBD titres in S1pr2-*Igk*$^{Tag/Tag}$ control mice immunized as in Fig. 2b,e, but not treated with tamoxifen. Graphs show median percentage of the anti-RBD titre that is $Strep^+$ ($(S/(S+F)*100)$) in the absence of tamoxifen at the pre-boost time point and two weeks after the second and third immunizations. This represents the median percentage by which $FLAG^+$ titres in recall responses are likely to be underestimated by spontaneous recombination by the S1pr2-CreERT2 driver. Data are from 8 mice from 2 independent experiments. (**e**) Comparison of primary addiction data shown in Fig. 2e,f, stratified by cohort and ipsilateral versus contralateral boost. The 4th cohort of mice is the homologously boosted group shown in Fig. 4b–e, depicted here by open circles. Bars represent the mean of log transformed titres, error bars are SEM. Data are from 16 mice from 4 independent cohorts. (**f**) Comparison of primary addiction between 3rd and 4th responses in 9 mice from 2 cohorts, based on data from Fig. 2e,f,h. Bars represent the mean of log transformed titres, error bars are SEM.

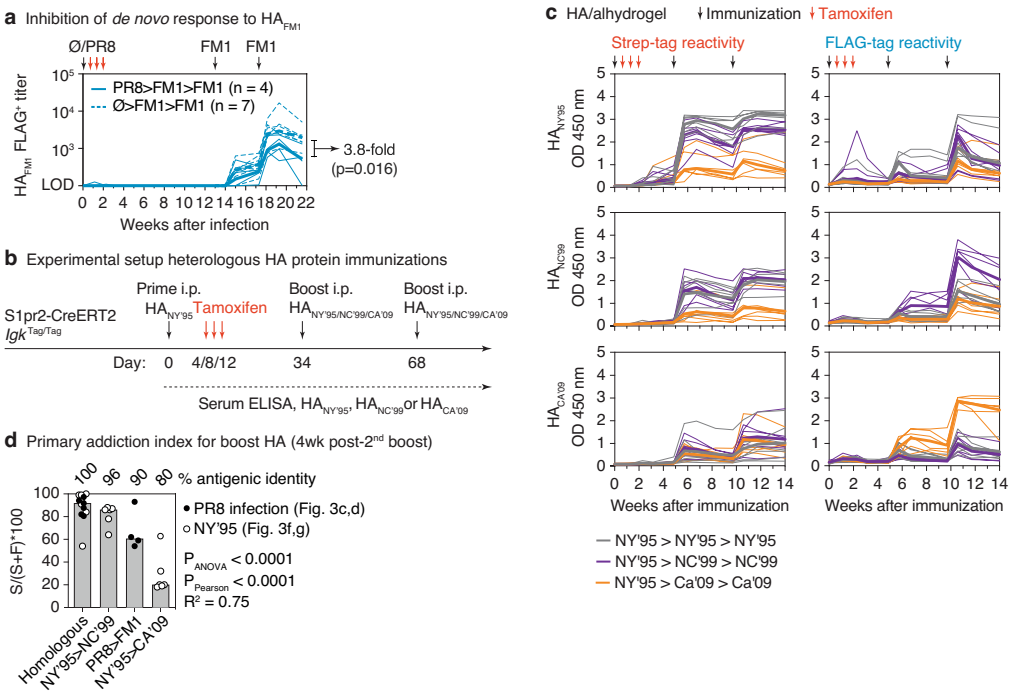

Extended Data Fig. 4 | Primary cohort recall upon heterologous HA protein boosting. (**a**) Comparison of *de novo* FLAG$^+$ antibody responses to HA_{FM1} in the presence or absence of primary infection with influenza virus PR8. PR8>FM1>FM1 data are for the same samples as in Fig. 3d, re-measured in the same assay as Ø>FM1>FM1. (**b**) Schematic representation of HA prime-boost strategy. S1pr2-*Igk*$^{Tag/Tag}$ mice were primed i.p. with HA_{NY95} in alhydrogel and boosted homologously or heterologously with HA_{N99} or HA_{CA09} in alhydrogel as indicated. (**c**) Full time course of anti-HA tag-specific ELISA reactivity (optical density at 1:100 dilution) of the same mice shown in Fig. 3f. Anti-HA_{NY95} (top), HA_{NC99} (middle) and HA_{CA09} (bottom) ELISAs are shown, with Strep (left) and FLAG (right) detection. (**d**) Relationship between primary addiction and antigenic distance for infection and immunization experiments. Graph compiles primary addiction indices from Fig. 3d and 3g. Bars are ordered by amino acid identity between the priming and boosting HAs. P-values are for one-way ANOVA, with % identity as a categorical variable, or Pearson correlation, with (100 – % identity) as a linear variable.

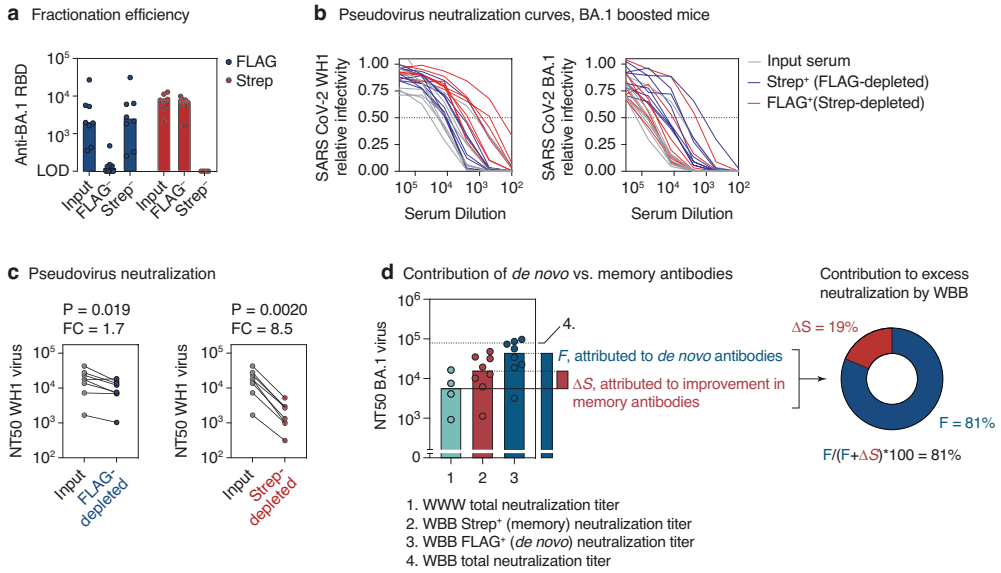

Extended Data Fig. 5 | Neutralization of WH1 and BA.1 pseudoviruses by serum antibody fractions from BA.1 boosted mice. (**a**) Efficiency of serum fractionation into FLAG and Strep-depleted fractions, as measured by anti-RBD ELISA of input vs. post-depletion samples. Serum was obtained from heterologously immunized mice two weeks after the 3rd immunization, Fig. 4d (8 mice from 2 independent experiments). (**b**) Neutralization of WH1 (left) and BA.1 (right) SARS-CoV-2 S-expressing pseudotyped HIV-1 virus by serum fractions shown in (a). Mean values of technical duplicates are shown. (**c**) WH1 S pseudovirus NT50 titres for samples in (b). Post-depletion NT50s were normalized to input serum based on the BA.1 RBD ELISA titres (a), by applying a correction equalizing the anti-RBD Strep-titre of the FLAG-depleted fraction to the input, and the anti-RBD FLAG-titre of the Strep-depleted fraction to the input. P-values are for one-tailed paired T test. FC, fold-change. (**d**) Estimating the contribution of *de novo* vs. memory-derived antibodies to excess BA.1 neutralization by the WBB regimen. The contribution of secondary affinity maturation or preferential selection of crossreactive memory B cells by BA.1 boosting, Δ*S*, is calculated as the difference between Strep$^+$ WBB and total WWW BA.1 neutralization titres (the latter are assumed to be all FLAG$^+$). The contribution of BA.1-specific antibodies induced *de novo* by BA.1 boosting, *F*, is given as the FLAG$^+$ WBB titre. Percent contribution of *F* to the improved BA.1 neutralization in WBB is calculated as (F/(F + ΔS))*100. Bars and dotted lines represent the medians for each condition, which were used to calculate F and ΔS. The upper dotted line (4.) represents the median neutralization of total WBB antibodies and is shown for reference purposes only. Data in groups 1 and 4 are reproduced from Fig. 4b, data in group 2 and 3 from Fig. 4h.

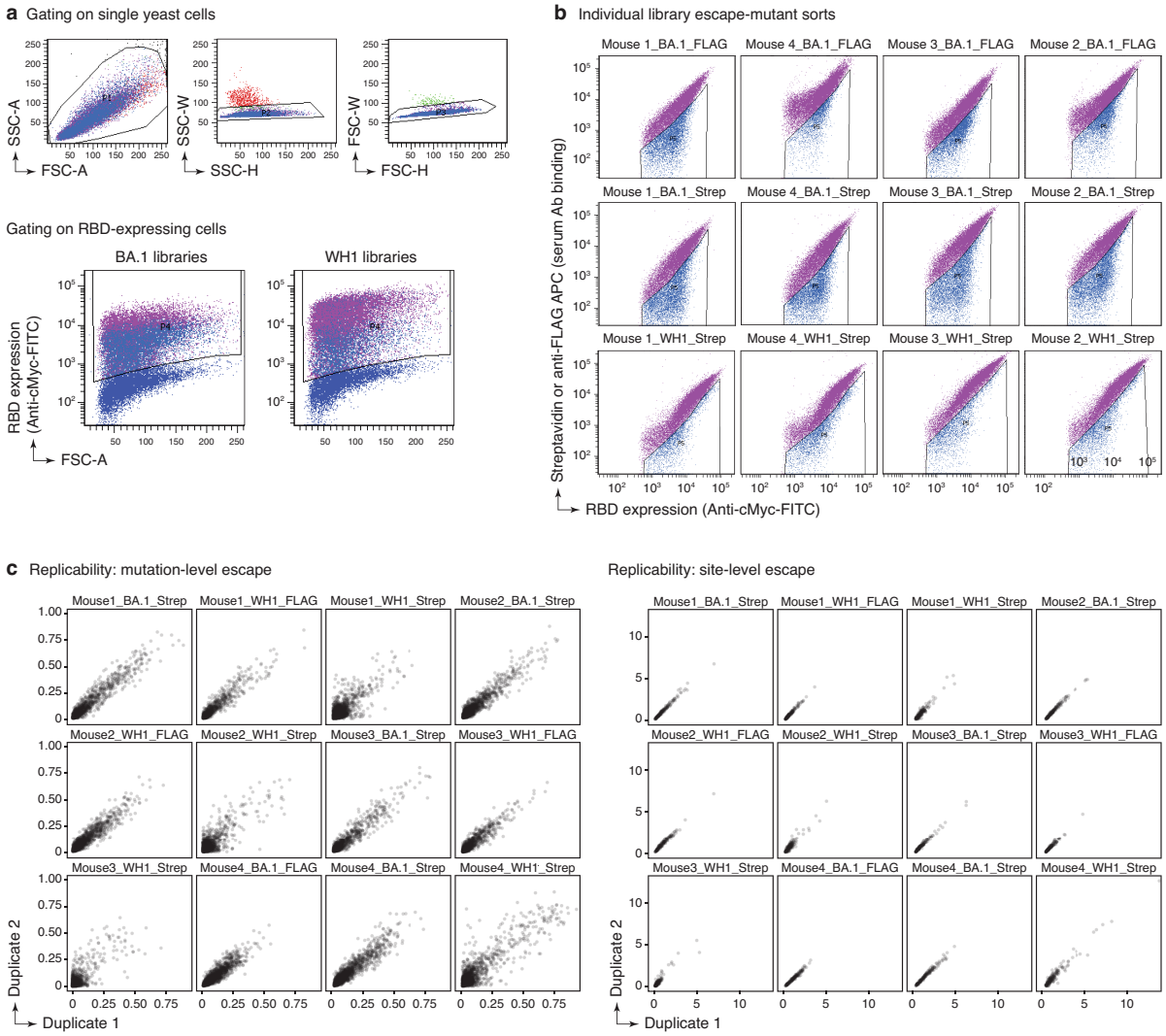

Extended Data Fig. 6 | Yeast-displayed deep mutational scanning to map mutations that reduce binding of immunized mouse serum. (**a**) Top: Representative plots of nested FACS gating strategy used for all experiments to select for single yeast cells. Bottom: Gating strategy to select for RBD-expressing single cells (FITC-A vs. FSC-A). (**b**) FACS gating strategy for one of two independent libraries to select cells expressing BA.1 or WH1 RBD mutants with reduced Strep or FLAG antibody binding (cells in blue), as measured by secondary staining with APC-conjugated streptavidin or APC-conjugated anti-FLAG antibody, respectively. Gates were set manually for each sample to capture cells that have a reduced amount of tagged antibody binding for their degree of RBD expression. FACS scatter plots were qualitatively similar between the two libraries. The mouse identifier (#1-4), DMS target library (WH1 or BA.1), and antibody tag (Strep or FLAG) are indicated above each plot. (**c**) Mutation (left)- and site (right)-level correlations of escape scores between two independent biological replicate libraries.

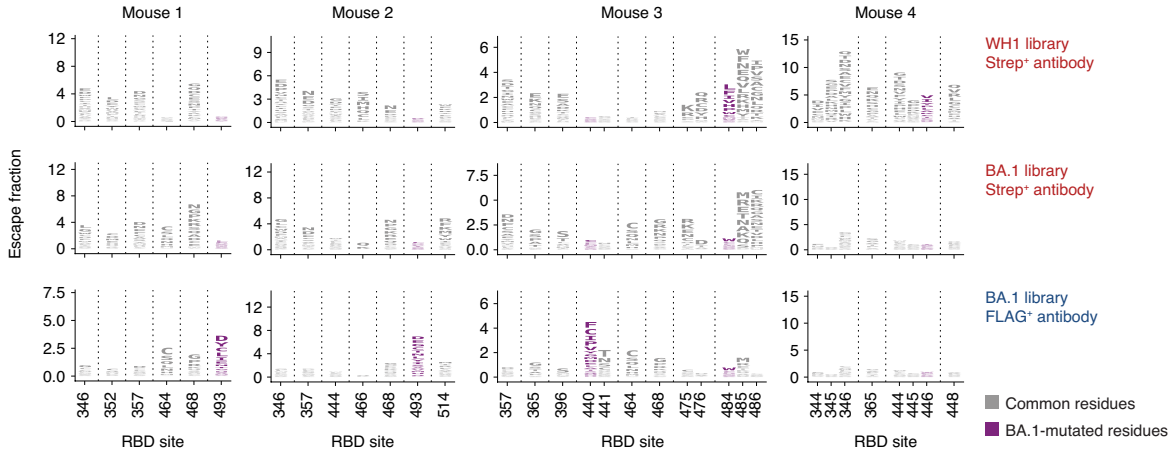

Extended Data Fig. 7 | RBD serum-escape logo plots. Deep mutational scanning results of serum collected from 4 heterologously immunized mice, 2 weeks after the 3rd dose (Fig. 4d). Each mutation's "escape fraction" was measured, which ranges from 0 (no cells effect on antibody binding) to 1 (all cells with the mutation have decreased antibody binding). Mouse 4 is not shown in the main text as there were no interpretable peaks in antibody binding to BA.1 libraries for either antibody fraction. Logo plots show the antibody-escape fractions for individual amino-acid mutations at key sites of strong escape. Sites in which BA.1 differs from the WH1 sequence are shown in purple font. All escape scores are shown in Supplementary Table 1 and are available online at https://github.com/jbloomlab/SARS-CoV-2-RBD_MAP_OAS/blob/main/results/supp_data/all_raw_data.csv.

nature portfolio

Corresponding author(s): G.D. Victora

Last updated by author(s): Jan 2, 2023

Reporting Summary

Nature Portfolio wishes to improve the reproducibility of the work that we publish. This form provides structure for consistency and transparency in reporting. For further information on Nature Portfolio policies, see our Editorial Policies and the Editorial Policy Checklist.

Statistics

For all statistical analyses, confirm that the following items are present in the figure legend, table legend, main text, or Methods section.

n/a	Confirmed	
☐	☒	The exact sample size (*n*) for each experimental group/condition, given as a discrete number and unit of measurement
☐	☒	A statement on whether measurements were taken from distinct samples or whether the same sample was measured repeatedly
☐	☒	The statistical test(s) used AND whether they are one- or two-sided *Only common tests should be described solely by name; describe more complex techniques in the Methods section.*
☐	☒	A description of all covariates tested
☐	☒	A description of any assumptions or corrections, such as tests of normality and adjustment for multiple comparisons
☐	☒	A full description of the statistical parameters including central tendency (e.g. means) or other basic estimates (e.g. regression coefficient) AND variation (e.g. standard deviation) or associated estimates of uncertainty (e.g. confidence intervals)
☐	☒	For null hypothesis testing, the test statistic (e.g. *F*, *t*, *r*) with confidence intervals, effect sizes, degrees of freedom and *P* value noted *Give P values as exact values whenever suitable.*
☒	☐	For Bayesian analysis, information on the choice of priors and Markov chain Monte Carlo settings
☒	☐	For hierarchical and complex designs, identification of the appropriate level for tests and full reporting of outcomes
☐	☒	Estimates of effect sizes (e.g. Cohen's *d*, Pearson's *r*), indicating how they were calculated

Our web collection on statistics for biologists contains articles on many of the points above.

Software and code

Policy information about availability of computer code

Data collection	Data collection code was not used in this study
Data analysis	Analysis of deep sequencing data is detailed in the methods section. We used the dms_variants package (https://jbloomlab.github.io/dms_variants/, version 1.4.0) to count each barcoded RBD variant in each pre-selection and serum-escape population. Full documentation of the computational analysis is at https://github.com/jbloomlab/SARS-CoV-2-RBD_MAP_OAS. The serum-escape map logo and line plots were created using the dmslogo package (https://jbloomlab.github.io/dmslogo, version 0.6.2). The code that generates these logo plot visualizations is available at https://github.com/jbloomlab/SARS-CoV-2-RBD_MAP_OAS/blob/main/results/summary/escape_profiles.md. To visualize serum escape on the RBD structure, the WH1 RBD surface (PDB 6M0J) was colored by the site-wise escape metric at each site, with white indicating no escape and red indicating the site with the most escape. Graphs were plotted using Prism v.9, and edited for appearance using Adobe Illustrator 27.1.1. Statistical tests were performed in Prism v.9. Flow cytometry data was analyzed using FlowJo v10.

For manuscripts utilizing custom algorithms or software that are central to the research but not yet described in published literature, software must be made available to editors and reviewers. We strongly encourage code deposition in a community repository (e.g. GitHub). See the Nature Portfolio guidelines for submitting code & software for further information.

Data

Policy information about availability of data

All manuscripts must include a data availability statement. This statement should provide the following information, where applicable:

- Accession codes, unique identifiers, or web links for publicly available datasets
- A description of any restrictions on data availability
- For clinical datasets or third party data, please ensure that the statement adheres to our policy

Renderings of Spike RBD and hemagglutinin structures were obtained from the Protein Data Bank (PDB), with accession codes PDB: 6MOJ (https://www.rcsb.org/structure/6m0j), PDB: 1RU7 (https://www.rcsb.org/structure/1RU7), PDB: 3LZG (https://www.rcsb.org/structure/3LZG).

The raw Illumina reads of the 16-nucleotide variant barcodes from the deep mutational scanning experiments are available on the NCBI SRA under BioProject PRJNA770094, BioSample SAMN30086726. All escape scores are shown in Supplemental Spreadsheet 1 and are available online at https://github.com/jbloomlab/SARS-CoV-2-RBD_MAP_OAS/blob/main/results/supp_data/all_raw_data.csv.

Code availability
The full code that analyzes the deep mutational scanning experiments is available at https://github.com/jbloomlab/SARS-CoV-2-RBD_MAP_OAS. The code that generates the logo plot visualizations is available at https://github.com/jbloomlab/SARS-CoV-2-RBD_MAP_OAS/blob/main/results/summary/escape_profiles.md.

Human research participants

Policy information about studies involving human research participants and Sex and Gender in Research.

Reporting on sex and gender	N/A
Population characteristics	N/A
Recruitment	N/A
Ethics oversight	N/A

Note that full information on the approval of the study protocol must also be provided in the manuscript.

Field-specific reporting

Please select the one below that is the best fit for your research. If you are not sure, read the appropriate sections before making your selection.

☒ Life sciences ☐ Behavioural & social sciences ☐ Ecological, evolutionary & environmental sciences

For a reference copy of the document with all sections, see nature.com/documents/nr-reporting-summary-flat.pdf

Life sciences study design

All studies must disclose on these points even when the disclosure is negative.

Sample size	No statistical methods were used to determine sample size. Numbers of mice per group within each independent experiment were limited to numbers typically used in the field.
Data exclusions	For pseudovirus neutralization curves, the mean of two technical duplicates is shown, gross outlier points likely resulting from experimental error were excluded as mentioned in the methods. For the HA NY'95 boosting experiment (Fig. 3f), one homologously-boosted mouse was excluded based on lack of evidence of proper serum fate-mapping.
Replication	Experiments were performed multiple times independently, as described in the figure legends. In some cases, results were stratified by cohort to show the consistency of results (Extended Data Fig. 3e).
Randomization	Littermate mice were divided stochastically between experimental groups to control for litter, cage, and age effects.
Blinding	Experimenters were not blinded to experimental group.

Behavioural & social sciences study design

All studies must disclose on these points even when the disclosure is negative.

Study description	*Briefly describe the study type including whether data are quantitative, qualitative, or mixed-methods (e.g. qualitative cross-sectional, quantitative experimental, mixed-methods case study).*
Research sample	*State the research sample (e.g. Harvard university undergraduates, villagers in rural India) and provide relevant demographic information (e.g. age, sex) and indicate whether the sample is representative. Provide a rationale for the study sample chosen. For studies involving existing datasets, please describe the dataset and source.*
Sampling strategy	*Describe the sampling procedure (e.g. random, snowball, stratified, convenience). Describe the statistical methods that were used to predetermine sample size OR if no sample-size calculation was performed, describe how sample sizes were chosen and provide a rationale for why these sample sizes are sufficient. For qualitative data, please indicate whether data saturation was considered, and what criteria were used to decide that no further sampling was needed.*
Data collection	*Provide details about the data collection procedure, including the instruments or devices used to record the data (e.g. pen and paper, computer, eye tracker, video or audio equipment) whether anyone was present besides the participant(s) and the researcher, and whether the researcher was blind to experimental condition and/or the study hypothesis during data collection.*
Timing	*Indicate the start and stop dates of data collection. If there is a gap between collection periods, state the dates for each sample cohort.*
Data exclusions	*If no data were excluded from the analyses, state so OR if data were excluded, provide the exact number of exclusions and the rationale behind them, indicating whether exclusion criteria were pre-established.*
Non-participation	*State how many participants dropped out/declined participation and the reason(s) given OR provide response rate OR state that no participants dropped out/declined participation.*
Randomization	*If participants were not allocated into experimental groups, state so OR describe how participants were allocated to groups, and if allocation was not random, describe how covariates were controlled.*

Ecological, evolutionary & environmental sciences study design

All studies must disclose on these points even when the disclosure is negative.

Study description	*Briefly describe the study. For quantitative data include treatment factors and interactions, design structure (e.g. factorial, nested, hierarchical), nature and number of experimental units and replicates.*
Research sample	*Describe the research sample (e.g. a group of tagged Passer domesticus, all Stenocereus thurberi within Organ Pipe Cactus National Monument), and provide a rationale for the sample choice. When relevant, describe the organism taxa, source, sex, age range and any manipulations. State what population the sample is meant to represent when applicable. For studies involving existing datasets, describe the data and its source.*
Sampling strategy	*Note the sampling procedure. Describe the statistical methods that were used to predetermine sample size OR if no sample-size calculation was performed, describe how sample sizes were chosen and provide a rationale for why these sample sizes are sufficient.*
Data collection	*Describe the data collection procedure, including who recorded the data and how.*
Timing and spatial scale	*Indicate the start and stop dates of data collection, noting the frequency and periodicity of sampling and providing a rationale for these choices. If there is a gap between collection periods, state the dates for each sample cohort. Specify the spatial scale from which the data are taken*
Data exclusions	*If no data were excluded from the analyses, state so OR if data were excluded, describe the exclusions and the rationale behind them, indicating whether exclusion criteria were pre-established.*
Reproducibility	*Describe the measures taken to verify the reproducibility of experimental findings. For each experiment, note whether any attempts to repeat the experiment failed OR state that all attempts to repeat the experiment were successful.*
Randomization	*Describe how samples/organisms/participants were allocated into groups. If allocation was not random, describe how covariates were controlled. If this is not relevant to your study, explain why.*
Blinding	*Describe the extent of blinding used during data acquisition and analysis. If blinding was not possible, describe why OR explain why blinding was not relevant to your study.*

Did the study involve field work? ☐ Yes ☒ No

Field work, collection and transport

Field conditions	*Describe the study conditions for field work, providing relevant parameters (e.g. temperature, rainfall).*
Location	*State the location of the sampling or experiment, providing relevant parameters (e.g. latitude and longitude, elevation, water depth).*
Access & import/export	*Describe the efforts you have made to access habitats and to collect and import/export your samples in a responsible manner and in compliance with local, national and international laws, noting any permits that were obtained (give the name of the issuing authority, the date of issue, and any identifying information).*
Disturbance	*Describe any disturbance caused by the study and how it was minimized.*

Reporting for specific materials, systems and methods

We require information from authors about some types of materials, experimental systems and methods used in many studies. Here, indicate whether each material, system or method listed is relevant to your study. If you are not sure if a list item applies to your research, read the appropriate section before selecting a response.

Materials & experimental systems

n/a	Involved in the study
☐	☒ Antibodies
☐	☒ Eukaryotic cell lines
☒	☐ Palaeontology and archaeology
☐	☒ Animals and other organisms
☒	☐ Clinical data
☒	☐ Dual use research of concern

Methods

n/a	Involved in the study
☒	☐ ChIP-seq
☐	☒ Flow cytometry
☒	☐ MRI-based neuroimaging

Antibodies

Antibodies used

1. B220-BV785, Biolegend Cat# 103246, clone RA3-6B2
2. CD4-V500, BD Biosciences Cat# 560782, clone RM4-5
3. CD8a-V500, BD Biosciences Cat# 560776, clone 53-6.7
4. CD38-APC, eBioscience Cat# 17-0381-82, clone 17-0381-82
5. Fas/CD95-PE/Cy7, BD Biosciences Cat# 557653, clone Jo2
6. CD138-BV650, Biolegend Cat# 142517, clone 281-2
7. FLAG (DYKDDDDK)-APC, Biolegend Cat# 637308, clone L5
8. FLAG (DYKDDDDK)-BV421, Biolegend Cat# 637322, clone L5
9. Strep-FITC, LS Bio Cat# LS-C203631-100, clone 5A9F9
10. IgLambda-BV421, BD Biosciences Cat# 744523, clone R26-46
11. IgLambda-FITC, BD Biosciences Cat# 553434, clone R26-46
12. IgA-PE, eBioscience Cat# 12-4204-82, clone mA-6E1
13. IgM-APC-eFluor 780, eBioscience Cat# 47-5790-82, clone II/41
14. IgM-PE/Cy7, eBioscience Cat# 25-5790-81, clone II/41
15. CD16/32-NA, Bio X Cell Cat# BE0307, clone 2.4G2
16. MYC-FITC, Immunology Consultants Lab Cat# CYMC-45F, polyclonal
17. Streptavidin-APC, Invitrogen Cat# S-868

Validation

All antibodies validated on the manufacturers website, see:
1. https://www.biolegend.com/en-us/products/brilliant-violet-785-anti-mouse-human-cd45r-b220-antibody-7960?GroupID=GROUP658
2. https://www.bdbiosciences.com/en-us/products/reagents/flow-cytometry-reagents/research-reagents/single-color-antibodies-ruo/v500-rat-anti-mouse-cd4.560782
3. https://www.bdbiosciences.com/en-eu/products/reagents/flow-cytometry-reagents/research-reagents/single-color-antibodies-ruo/v500-rat-anti-mouse-cd8a.560776
4. https://www.thermofisher.com/antibody/product/CD38-Antibody-clone-90-Monoclonal/17-0381-82
5. https://www.bdbiosciences.com/en-eu/products/reagents/flow-cytometry-reagents/research-reagents/single-color-antibodies-ruo/pe-cy-7-hamster-anti-mouse-cd95.557653
6. https://www.biolegend.com/en-us/products/brilliant-violet-650-anti-mouse-cd138-syndecan-1-antibody-8800?GroupID=BLG9623
7. https://www.biolegend.com/en-us/products/apc-anti-dykddddk-tag-antibody-8099?GroupID=GROUP26
8. https://www.biolegend.com/en-us/products/brilliant-violet-421-anti-dykddddk-tag-antibody-16139
9. https://www.lsbio.com/antibodies/strep-tag-ii-antibody-clone-5a9f9-fitc-flow-icc-if-immunofluorescence-ls-c203631/211887
10. https://www.bdbiosciences.com/en-us/products/reagents/flow-cytometry-reagents/research-reagents/single-color-antibodies-ruo/bv421-rat-anti-mouse-ig-1-2-3-light-chain.744523
11. https://www.bdbiosciences.com/en-us/products/reagents/flow-cytometry-reagents/research-reagents/single-color-antibodies-

ruo/fitc-rat-anti-mouse-ig-1-2-3-light-chain.553434
12. https://www.thermofisher.com/antibody/product/IgA-Antibody-clone-mA-6E1-Monoclonal/12-4204-82
13. https://www.thermofisher.com/antibody/product/IgM-Antibody-clone-II-41-Monoclonal/47-5790-82
14. https://www.thermofisher.com/antibody/product/IgM-Antibody-clone-II-41-Monoclonal/25-5790-82
15. https://bioxcell.com/invivoplus-anti-mouse-cd16-cd32-bp0307
16. https://www.icllab.com/anti-c-myc-antibody-chicken-fitc-conjugated-cmyc-45f.html
17. https://www.thermofisher.com/order/catalog/product/S868

Eukaryotic cell lines

Policy information about cell lines and Sex and Gender in Research

Cell line source(s)	293F cell line was used for antibody production. Obtained from Thermo Fisher Scientific Cat# R79007.
Authentication	Since the cell lines were only used for protein production (which was confirmed as successful), no further authentication was performed.
Mycoplasma contamination	Cell lines tested negative for mycoplasma.
Commonly misidentified lines (See ICLAC register)	No commonly misidentified cell lines were used.

Animals and other research organisms

Policy information about studies involving animals; ARRIVE guidelines recommended for reporting animal research, and Sex and Gender in Research

Laboratory animals	6-12 week old adult male and female mice on the C57BL/6J background were used. See 'mice' section in the methods for further details. Mice were housed at 72 °F and 30–70% humidity in a 12-h light/dark cycle with ad libitum access to food and water.
Wild animals	The study did not involve wild animals.
Reporting on sex	Both sexes of mice were used throughout the study. No significant differences were noted between sexes.
Field-collected samples	The study did not involve samples collected from the field.
Ethics oversight	All mouse procedures were approved by the Rockefeller University's Institutional Animal Care and Use Committee

Note that full information on the approval of the study protocol must also be provided in the manuscript.

Flow Cytometry

Plots

Confirm that:

☒ The axis labels state the marker and fluorochrome used (e.g. CD4-FITC).

☒ The axis scales are clearly visible. Include numbers along axes only for bottom left plot of group (a 'group' is an analysis of identical markers).

☒ All plots are contour plots with outliers or pseudocolor plots.

☒ A numerical value for number of cells or percentage (with statistics) is provided.

Methodology

Sample preparation	For flow cytometry of peripheral B cells, blood was collected in microtubes with EDTA to prevent coagulation and treated with ACK buffer to lyse red-blood cells. For lymph node samples, cell suspensions were obtained by mechanical disassociation with disposable micropestles. Spleens were homogenized by filtering through a 70-µm cell strainer and treated with ACK buffer. Bone-marrow cells were extracted by centrifugation of punctured tibiae and femurs at up to 10,000 xG for 10 s, then treated with ACK buffer. Cells from each tissue were resuspended in PBS supplemented with 0.5% BSA and 1 mM EDTA.
Instrument	BD FACS Symphony cytometer
Software	FlowJo v.10 software
Cell population abundance	No cell sorting was performed except of yeast libraries for deep mutational scanning, as detailed in the methods section and shown in Extended Data Fig. 6.
Gating strategy	See figures and legends for detailed description. In brief, we gated on single lymphocytes using forward and side scatter. T cells as defined by CD4 and CD8 expression were first gated out. B cells were then defined as B220+CD138–, whereas plasma cells where defined as B220low, CD138high (see Extended Data Fig. 2c). GC B cells were gated as FAS+CD38– as shown in Fig. 1e and Extended Data Fig. 2f. For bone marrow, plasma cells were gated as IgA+ and IgL– as in Extended Data Fig. 2c. FLAG

and Strep-tag gating is shown in Fig. 1b,e and Extended Data Fig. 2a,c,f. Gating strategies for yeast library sorting are detailed in Extended Data Fig. 6.

☒ Tick this box to confirm that a figure exemplifying the gating strategy is provided in the Supplementary Information.